Brake wear particle emissions from heavy-duty vehicles and their environmental implication

Freja Wirén & Olga Schubert

DIVISION OF ERGONOMICS AND AEROSOL TECHNOLOGY | DEPARTMENT OF DESIGN SCIENCES
FACULTY OF ENGINEERING LTH | LUND UNIVERSITY
2026

MASTER THESIS

Lund University



Brake wear particle emissions from heavy-duty vehicles and their environmental implication

Freja Wirén & Olga Schubert



LUND
UNIVERSITY

Brake wear particle emissions from heavy-duty vehicles and their environmental implication

Copyright © 2026 Freja Wirén & Olga Schubert

Published by
Department of Design Sciences
Faculty of Engineering LTH, Lund University
P.O. Box 118, SE-221 00 Lund, Sweden

Subject: Aerosol Technology (MAMM05),
Division: Division of Ergonomics and Aerosol Technology, Department of Design Sciences, Faculty of Engineering LTH, Lund University
Supervisor: Yezhe Lyu
Co-supervisor: Jens Wahlström & Joakim Pagels
Examiner: Axel Eriksson

Abstract

Today, non-exhaust emissions from brake wear are one of the biggest sources of air polluting PM_{10} in urban areas. To limit toxic effects, the recent Euro 7 regulations include non-exhaust emissions limit values for passenger cars. However, regulatory standards for heavy-duty vehicles (HDVs) do not yet exist and the effects of brake wear particles from HDVs are underexplored. The aim of this thesis is therefore to improve the understanding on HDV brake wear particles and their environmental implications. Using a Pin on Disc tribometer, brake wear from three different HDV brake pads were generated and collected for analysis of elemental composition and cell toxicity. Also, online measurements of particle emissions were made. The results demonstrate the brake wear particles to mainly be in the fine particles size range, and no formation of ultrafine particles were found. Moreover, the brake pads with the lowest brake emissions showed sign of high toxicity, which was linked to the high copper content found in these brake wear particles. Additionally, non-airborne particles were found to contain less aluminium and more heavy metals compared to airborne particles. In conclusion, brake particles from HDVs pose an environmental risk, as the fine particles are subject to high dispersion and have more severe health effects. At the same time, the depositing particles pose a risk of contaminating aquatic environments and soil. This questions the use of only PM_{10} regulations to limit negative effects, since it does not take elemental toxicity into consideration. Further research is needed to understand the toxic effects and formation of brake wear particles from HDVs.

Keywords: Particle emissions, Brake wear, Aerosol, Non-exhaust emissions, Toxicity, Heavy-duty vehicles

Sammanfattning

Idag är partikelutsläpp från bromsslitage en av de största källorna till luftförorenande PM_{10} i stadsområden. För att begränsa negativa effekter inkluderar den senaste Euro 7-förordningen gränsvärden för slitagepartiklar från bromsar i lättviktsfordon. Dock saknas fortfarande liknande reglering för tunga fordon, samtidigt som forskningen är begränsad. Syftet med den här rapporten är därför att undersöka partikelutsläpp från bromsslitage från just tunga fordon samt dess miljö- och hälsopåverkan. Med hjälp av en Pin on Disc tribometer genererades partiklar från tre olika bromsbelägg för tunga fordon, som samlades in och analyserades för ämneskomposition samt toxicitet. Även online-mätningar gjordes för att kartlägga utsläppsmönster från bromsbeläggen. Resultaten visar att majoriteten partiklar från samtliga bromsbelägg befinner sig inom storleksintervallet för $PM_{2.5}$, men att inga ultrafina partiklar kunde påvisas. Däremot visade sig det bromsbelägg med lägst partikelutsläpp ha högst toxicitet. Detta bromsbelägg innehöll också störst mängd koppar, vilket identifierades som orsak till både de låga utsläppen och toxiciteten. Dessutom konstaterades det att de icke-luftburna utsläppen innehöll mer tungmetaller än de luftburna. Sammanfattningsvis dras slutsatsen att det finns miljö- och hälsorisker med bromspartiklar från tunga fordon. Detta eftersom $PM_{2.5}$ både anses ha stor spridningsförmåga och orsaka störst negativa hälsoeffekter. Samtidigt utgör icke-luftburna partiklar en risk att förorena jord och akvatiska miljöer. Därmed ifrågasätter denna studie reglering av utsläpp med endast PM_{10}, eftersom den varken tar hänsyn till partiklarnas toxicitet eller de icke-luftburna. Fortsatt forskning krävs för att djupare förstå hur bromspartiklar från tunga fordon bildas och har för effekter.

Nyckelord: Partikelutsläpp, Bromsslitage, Aerosoler, Icke-avgasutsläpp, Toxicitet, Tunga fordon

Acknowledgments

This thesis would not have been completed without the help and guidance we have received along the way. We would like to express our sincerest appreciation for the whole team at Keio University Environmental Chemistry lab for welcoming us in their laboratory and office. This includes professor Tomoaki Okuda who as the international host gave us a warm welcome and took excellent care of us during our stay, but also assistant professor Raga Ishikawa for taking the time and effort to analyse the toxicity studies, as well as MSc student Ryutaro Hirabashi for helping us with the EDXRF analysis. Moreover, we want to express our gratitude to the Erasmus+ International Credit Mobility programme and Scandinavia-Japan Sasakawa Foundation, as without their financial support this exchange would not have been possible.

Throughout the thesis process we have received the best possible support from our supervisors, and we thank Jens Wahlström and Joakim Pagels for taking the time from their busy schedule to guide and help us.

Last but certainly not least, we say the greatest possible thank you to our incredible lead supervisor Yezhe Lyu. It is thanks to his knowledge, guidance and unwavering support that this thesis work could be completed.

Lund, June 2026

Freja Wirén & Olga Schubert

Table of contents

List of acronyms and abbreviations 9
1 Introduction 10
1.1 Motivation 10
1.2 Aims and Objectives 11
2 Theoretical background 12
2.1 General characteristics of airborne particles and particulate matter 12
2.2 Brake wear particles and non-exhaust emissions 13
2.2.1 Generation of brake wear particles 15
2.2.2 Characteristics of brake wear particles 16
2.3 Health and environmental effects of brake wear particles 16
2.4 Experimental Methods 19
2.4.1 Pin on Disc Tribometer 19
2.4.2 Particulate Matter measurement instruments 19
2.4.3 Energy Dispersive X-ray Fluorescence Spectrometry 21
2.4.4 Water Soluble Tetrazolium Assay 21
2.4.5 Detection of Intracellular Reactive Oxygen Species 22
3 Materials and design of experiments 23
3.1 Materials 23
3.2 Online Analysis 24
3.3 Collection of particles 27
3.4 Offline analysis 28
3.4.1 Particle elemental composition 28
3.4.2 Cell exposure tests 29
4 Results and discussion 33
4.1 Particle collection 33
4.2 Online analyses of particulate matter 34
4.2.1 PM_{10} concentration 34
4.2.2 Particle number concentration 37

4.2.3 Particle size distribution 40
4.2.4 General discussion online measurements 42
4.3 Offline Measurements 44
4.3.1 Particle elemental composition 44
4.3.2 Cell toxicity 46
4.3.3 General discussion offline measurements 50
4.4 Uncertainties and Limitations 51
5 Environmental implication 53
5.1 Conclusion 54
5.2 Future research 55
6 References 56
Appendix A Brake mechanics 61
Appendix B Online data 62
B.1 PM_{10} (MiniWRAS) 62
B.1.1 PM_{10} concentration repetitions 62
B.1.2 Calculation of average PM_{10} concentration based on sample mass 64
B.2 Particle number concentration (CPC) 64
B.3 Particle size distribution (MiniWRAS & SMPS) 65
B.3.1 Particle size distribution repetitions 65
B.3.2 Size distribution analysis of PNC peaks 69
Appendix C Metal composition of particles (EDXRF) 70
C.1 Relative elemental composition. Water soluble filter with airborne particles. 70
C.2 Relative elemental composition. Teflon filter with non-airborne particles. 71
Appendix D Cell exposure data 72
D.1 Cell viability data 72
D.1.1 Calculations of relative cell viability 72
D.1.2 WST-1 assay results, n=4 73
D.2 ROS production data, n=4 73

List of acronyms and abbreviations

BWP	Brake Wear Particles
CPC	Condensation Particle Counter
EEA	European Environmental Agency
EDXRF	Energy Dispersive X-ray Fluorescence
EPA	Environmental Protection Agency
HDV	Heavy-duty Vehicle
LDV	Light-duty Vehicle
MEM	Minimum Essential Media
MiniWRAS	Mini Wide-range Aerosol Spectrometer
NEE	Non-exhaust Emissions
PM	Particulate Matter
PNC	Particle Number Concentration
PoD	Pin on Disc
ROS	Reactive Oxygen Species
RPM	Rounds per Minute
SMPS	Scanning Mobility Particle Sizer
WHO	World Health Organization
WST	Water Soluble Tetrazolium
XRF	X-ray Fluorescence

1 Introduction

1.1 Motivation

Air pollution is one of the largest environmental issues today and a threat to human health. A major contributor to air polluting emissions is the transport sector, partially due to combustion exhaust but also wear of tires, roads and brakes, the so-called non-exhaust emissions (NEE). As exhaust emissions decrease due to European emissions regulatory standards, increased usage of electric cars and alternative fuels, the impact of NEE is rising and already exceeds exhaust emissions in some countries. Additionally, current development of the global vehicle fleet further increases the contribution of NEE, since the number of vehicles is increasing as well as becoming heavier due to electrification (Harrison et al., 2021; Wahlström et al., 2025).

One of the most significant sources of NEE is brake wear particles (BWP). Brake wear particles are contributing up to 55% of total NEE in urban areas and seems to be more toxic compared to other air pollution sources (Christou et al., 2025). Consequently, humans are highly exposed to these emissions, both through inhalation of airborne particles, but also from uptake of polluted soil or water by non-airborne deposited particles (Grigoratos & Martini, 2015).

In order to combat such effects, the Euro 7 regulation, adopted by the European Council, are presenting the first limit values for brake wear PM_{10} emissions for light-duty vehicles (LDVs). However, no similar reference values are introduced for heavy-duty vehicles (HDVs) (2024/1247/EG). In contrast to LDVs, demand more intense braking and therefore brake pads with a higher metal content, which elements potentially have toxic effects on both environment and human health (Forest & Pourchez, 2023).

Brake wear emissions from HDVs are today underexplored and knowledge of its particles and their effects are largely limited. The aim of this master's thesis is therefore to improve the understanding on BWP from HDVs and thereby provide a base for future studies and regulatory standards for these emissions.

1.2 Aims and Objectives

The aim of this master's thesis is to evaluate the possible environmental and health implications of brake wear particle emissions from heavy-duty vehicles. In order to achieve this, a comparative study was made on brake wear particles from three different brake pad materials for heavy-duty vehicles. The following investigations were performed:

- Particle number concentration, PM_{10} concentration and size distribution.
- Particle elemental composition.
- Cell toxicity analyses.

2 Theoretical background

2.1 General characteristics of airborne particles and particulate matter

Particulate matter (PM) is defined as solid or liquid particles. PM can become airborne through suspension in gas, usually air, and is then defined as aerosol particles. The majority of aerosol particles are from natural origin, such as sea spray or wildfire ash, however, anthropogenic activities can make up to about 60% of all airborne PM in urban areas. Such activities are mainly from wood burning, industry or transport (Sjöberg, et al., 2023). According to the World Health Organization (WHO), PM is such a common air polluter that it is a proxy indicator for poor air quality (WHO, 2024).

The categorization of airborne PM is mainly done by size, using three fractions of particle diameter: coarse particles (diameter 10-2.5 μm), fine particles (diameter < 2.5 μm) and ultrafine particles (diameter < 0.1 μm). Fine and ultrafine particles are additionally defined as $PM_{2.5}$ and $PM_{0.1}$ respectively, while PM_{10} refers to all particulate matter smaller than 10 μm, i.e. all three fractions. The relative size comparison between particle fractions is illustrated in Figure 1.



Figure 1: Particle size comparison if the particles were 30 000 times larger (Sjöberg et al., 2023)

The size of particles strongly influences air suspension time and how fast they settle on the ground. Settling velocity for particles is found through Equation 1 (a correction factor is required for diameter less than 1 μm) (Hinds, 1999).

$$Settling\ velocity = \frac{\rho * d^2 * g}{18 * \eta}\ , d > 1\ \mu m, Re < 1.0 \qquad (1)$$

As can be seen in equation 1, the settling velocity additionally depends on both particle density and the viscosity of the surrounding media (η). However, since

settling velocity is proportional to the square of particle diameter, this property has the largest impact on particle deposition. Therefore, the fastest settling particles are from the coarse fraction, being the largest, while fine and ultrafine particles can stay air suspended for a longer time. Moreover, the particle fractions have different origins. Coarse particles are mainly created from mechanical processes such as erosion or abrasion of materials, while fine and ultrafine particles mostly originate from chemical processes, such as combustion. However, some processes generate all three fractions, such as atmospheric processes as well as wear of brakes and tyres (Sjöberg et al., 2023).

To limit negative environmental effects from airborne particles, air quality guidelines and legislation are implemented. According to the EU Ambient Air Quality Directive, the limit values for exposure of $PM_{2.5}$ and PM_{10}, as an average over one year, is 25 $\mu g/m^3$ and 40 $\mu g/m^3$ respectively. This directive especially points out fine particulate matter ($PM_{2.5}$-$PM_{0.1}$) as the main air pollutant (2024/2881/EG). Additionally, there are legislations to specifically limit traffic related emissions, such as the Euro 7 regulation. This regulation is solely aimed at road transport and recently the environmental impact from both exhaust emissions and NEE. The limit values of brake wear PM_{10} emissions for all LDVs are 7 mg/km driven vehicle, except for electric vehicles with 3 mg/km. Updated limit values, which also include HDVs, are not presented until 2030 (2024/1247/EG).

2.2 Brake wear particles and non-exhaust emissions

The previous main contributor to transport related air pollution, tail pipe exhaust emissions, is today being passed by non-exhaust emissions in many countries. According to the European Environmental Agency (EEA), the contribution to PM_{10} and $PM_{2.5}$ from NEE within road transport of the EU-27 countries was equal to 77%, and 60% respectively during 2023. As this percentual share continues to rise, the impact of NEE is increasing (EEA, 2025). Similar results were presented by Järlskog & Gustavsson, which reported in 2021 and 2022 that only 6% of Sweden´s road transport emissions were attributed to exhaust emissions. The majority was instead NEE from tyres, brakes and road material (Järlskog & Gustavsson, 2023).

Out of these NEEs, the main contributor to PM is brake wear. According to measurements made by EU funded EIT Urban Mobility, it was found that between 2017 and 2021, brake wear emissions accounted for 41% of the combined PM_{10} from brake, tyre and road wear, which was higher than for any of the other two (EIT Urban Mobility, 2025). This conclusion has also been made by London Atmospheric Emissions Inventory (2025), which found that the PM_{10} contributions from brake wear in greater London was significantly larger than wear from tyres or exhaust emissions (EIT Urban Mobility, 2025).

Naturally, the origin of brake wear NEE are particles released during a braking incidence. There are two different types of brake systems widely used today, drum brakes and disc brakes. Both systems rely on friction to operate between either drum and shoe, or disc and pad, as illustrated in Figure 2. According to EIT Urban Mobility (2025), drum brakes have proven to be a better alternative with respect to air pollution, resulting in about 23% less wear than disc brakes. However, due to the higher braking performance of the disc brakes, these are more commonly used. This applies both to LDVs and HDVs (EIT Urban Mobility, 2025). The brakes mainly used for HDVs are of the semi-metallic variety, as these are more capable of withstanding the higher temperatures associated with a higher braking force. For the disc brake systems, the disc is usually made of grey cast iron. (Grigoratos & Martini, 2015)

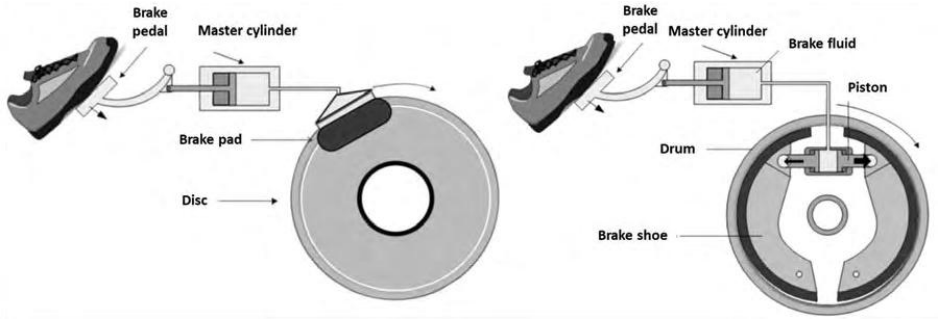


Figure 2: Disc brake system (left) and drum brake system (right) (EIT Urban Mobility, 2025).

HDVs are defined by the European Commission as vehicles weighing over 3.5 tonnes e.g. trucks. In addition, this category also includes passenger transport vehicles that seat more than 8 people such as buses in public transport or coaches (European Commission, 2014). Regarding NEE, HDVs have been found to emit 20% to three times more PM_{10} compared to LDVs, depending on the vehicle type. (Couval et al., 2026; EIT Urban Mobility, 2025). However, there is today no standardized testing protocol for HDVs, as there is for LDVs. As a result, there is a significant gap in research regarding HDVs, and existing information is mostly based on earlier studies on LDVs (EIT Urban Mobility, 2025). One such study is the extensive review made by Grigoratos and Martini in 2015, which to this day still is one of the most cited reports on BWP emission. Consequently, BWP from HDVs are understudied, and previous knowledge is limited. Nonetheless, there are some findings of LDV BWP that are likely applicable to particles from HDVs.

2.2.1 Generation of brake wear particles

Generation of BWP is the result of several processes. It is a complex combination of mechanisms of surface contact, friction and chemical reactions, including mechanical abrasion, thermal fatigue, thermal degradation, as well as tribo-oxidation. Depending on the process, different particle sizes are generated. For example, mechanical abrasion tends to generate larger particles compared to thermal fatigue and thermal degradation (EIT Urban Mobility, 2025). Moreover, as the temperature increases, the generation of BWP has been found to reach a transition temperature, also called critical temperature, where the formation of UFP drastically increases. However, the identified temperature differs and ranges between 150-300 °C depending on study and material (Couval et al., 2026; Perricone et al., 2019). Consequently, the resulting size distribution is a combination of particles from the different generation processes, but the influence of the temperature is still unclear.

Furthermore, the generated size distribution, as well as particle number concentration (PNC), is additionally affected by the driver's behaviour, mainly though more frequent and intensive braking. Intensive braking is achieved by increased sliding velocity as well as higher contact pressure, meaning braking with at higher velocity with greater force. This type of braking generally generates a higher amount of wear as well as larger particles (Hussain et al., 2014). As a result, brake wear is a large pollution source in urban settings, where vehicles drive more irregularly and has a higher frequency of braking occurrences (EIT Urban Mobility, 2025). The contribution of brake wear to total NEE in urban areas is roughly equal to 16-55%, whereas this number is significantly lower at highways (~3%), where braking occurrences are fewer (Grigoratos & Martini, 2015).

However, if brakes are not used for a period of time, corrosion occurs on the brake pad and break disc surfaces, making them rougher. This results in higher abrasion when braking eventually takes place, leading to a higher initial generation of BWP. This early time interval of increased wear is called the bedding period or running in period. It has been shown that for completely unused materials, the bedding period is the longest and results in the largest increase of particle emissions, before decreasing and reaching a steady state (Gramstat et al., 2020; Wang, 2025).

Moreover, the weight of the vehicle itself also plays a substantial role in brake particle formation. As heavier vehicles require larger braking force, the PM emissions increase almost linearly with the weight. As a result, HDVs are more prone to emit BWP (EIT Urban Mobility, 2025). Additionally, electrified vehicles are also expected to release more BWP due to the higher weight (EIT Urban Mobility, 2025; EEA, 2025). However, regenerative braking in electric vehicles may counteract this by limiting hard braking occurrences (EIT Urban Mobility, 2025). Other influencing factors include environmental conditions such as temperature and humidity (EIT Urban Mobility, 2025; Grigoratos & Martini, 2015).

2.2.2 Characteristics of brake wear particles

Once BWP are released, they will be dispersed in different ways and in different sizes. It has been found that 40-50% of the particles become air suspended, of which 80% is classified as PM_{10} (Grigoratos & Martini, 2015; EIT Urban Mobility, 2025). These particles are mainly expected to belong in the course particle fraction, as recorded by EIT Urban Mobility (2025), where the part of $PM_{2.5}$ present in the PM_{10} is equal to roughly 35-45%. However, according to Grigoratos & Martini (2015), several previous studies have also found high particle concentrations in both fine and ultrafine fractions, and that the resulting brake wear particles are generally smaller than other wear particles, such as road and tyre wear (Järlskog & Gustavsson, 2023).

Furthermore, composition of BWP varies due to large variety of brake types. Brake pad lining contains several different components, such as fillers, fibres, frictional additives, lubricants and abrasives, with common elements such as Ba, Pb, Cu, Zn, Cr and Fe (Grigoratos & Martini, 2015; EIT Urban Mobility, 2025). Brake pads with higher amount of Cu have been proven to produce lower emitted PM_{10} concentration as well as lower PNC (Lyu et al., 2020). This is caused by the high thermal conductivity and ductile properties of Cu, which is why it is commonly used as a reinforcing fibre in brake pads (Straffelini et al., 2015; Verma et al., 2015).

Consequently, Cu is more commonly found in HDV BWP compared to LDV. This is due to the need of increased brake performance of HDVs. Other elements found in the airborne BWP are similar to the brake pad content, such as Fe, Zn, Sn and Sb (EIT Urban Mobility, 2025). However, previous studies have found the iron content in such emissions to be dominating the metallic fraction, often equal to or succeeding 50% of heavy metals for both PM_{10} and $PM_{2,5}$ (Grigoratos & Martini, 2015; Lopez et al., 2023; Neukirchen et al., 2025).

2.3 Health and environmental effects of brake wear particles

Non-exhaust emissions from road transport have been identified to exhibit negative impacts on both health and environment (Grigoratos & Martini, 2025). Specifically brake particles are in general more toxic compared to other air pollution sources (Christou et al., 2025). This toxicity is influenced by several factors, with the most important ones being chemical composition, particle size and particle concentration. (Christou et al., 2025; Forest and Pourchez, 2023; Grigoratos & Martini, 2015).

An extensive review on health effects from brake wear, made by Forest and Pourchez (2023), concluded that brake particles could potentially cause oxidative stress, inflammation and DNA-damages. The studies that show this are mainly *in*

vitro, made on cells such as epithelial lung cells (Forest & Pourchez, 2023). However, epidemiological or *in vivo* studies are few and the only response shown by the existing ones is inflammation. This is supported by a more recent review, which also points out the lack of environmental studies as well as research on wear from HDVs (Christou et al., 2025).

Nonetheless, the present literature finds the toxic responses mainly linked to the chemical composition of the brake wear, especially the metal content (Christou et al., 2025; Forest & Pourchez, 2023). Some common metals found in BWP, such as Fe, Cu, Cr and Ni, are known to catalyse production of reactive oxygen species (ROS). ROS are naturally occurring, with vital functions in the body but can cause oxidative stress if overloaded. Oxidative stress is a degenerative process which can promote cardiovascular diseases, diabetes, cancer and neurodegeneration, possibly leading to diseases like Alzheimer´s or Parkinson´s (Ansari et al., 2025; Jomova et al., 2012). Additionally, other metals present, such as Zn, Al and Pb, can increase these effects. Moreover, several metals found in BWP have additional intrinsic toxic properties. Especially toxic for both humans and other species are heavy metals, of which Pb, Fe, Cu and Cr are found in BWP (Grigoratos & Martini, 2015). While Pb is acute cytotoxic, the other metals toxicity depends on both dose and chemical form, since this decides uptake and transport in the body (Christou et al., 2025; Sterner, 2010). Therefore, exposure to BWP alone is not necessarily toxic, and particle concentration is also an important factor to assess. Consequently, there is a possibility that semi-metallic brakes have a more negative impact to health and environment compared to brakes with lower metal content.

In addition, toxicity is related to particle size. As described, most of the particles in brake wear is PM_{10}, which is a part of the inhalable fraction. Depending on size, inhaled particles will end up in different parts of the body, influencing the health response. Coarse particles (PM_{10}-$PM_{2.5}$) will deposit in the upper parts of the respiratory tract, potentially causing irritation or asthmatic responses while fine ($PM_{2.5}$) and ultrafine ($PM_{0.1}$) particles reach deeper in the lungs (Karlsson, 2023). Here, brake wear could induce earlier described responses (oxidative stress, inflammation etc.) and according to Karlsson (2023), most health risks with aerosols are associated with $PM_{2.5}$. Moreover, ultrafine particles may penetrate all the way to the alveolar region, potentially enter the blood stream and spread to other parts of the body such as liver, kidneys and brain. Additionally, since ultrafine particles are smaller, the reactive surface is larger, which increases the possibility of toxic responses (Grigoratos & Martini, 2015). As a result, the relatively large share of fine particles in BWP poses a high risk of respiratory effects.

Furthermore, particle size strongly influences dispersion of BWP, which affects the exposure to it. According to Grigoratos and Martini (2015), 35-40% of the air suspended PM_{10} are fine particles, which have a lower settling velocity and therefore stay airborne for a longer time compared to larger particles (Equation 1). Consequently, a large part of the generated BWP has a high dispersion. The larger non-airborne particles will instead deposit close to the road or get stuck on the

vehicle. As a result, these non-airborne particles can theoretically be washed away by rain and surface water, potentially polluting aquatic environments but also contaminating sediments or plants. Additionally, deposited particles can be resuspended into the air and further dispersed and potentially inhaled (Grigoratos & Martini, 2015) (Figure 3).



Figure 3: Illustration of brake wear particle dispersion in the environment (Järlskog & Gustavsson, 2023).

To summarise, there are signs of cytotoxicity in exposure to BWP, which pose a risk of causing several severe conditions and diseases. According to *in vitro* studies, these responses are heavily related to the metal content, suggesting that BWP from HDVs are potentially more harmful compared to those from LDVs. Additionally, particle size and concentration decide the exposure in real life and are therefore also important factors to consider. However, as the literature points out, there are no comprehensive or epidemiological studies linking BWP specifically to these health effects, and there is a lack of specific studies, such as on HDV (Christou et al., 2025; Forest & Pourchez, 2023).

2.4 Experimental Methods

This section is dedicated to explaining the purpose and workings of the different methods and instruments used in sampling and analysing the brake wear particles.

2.4.1 Pin on Disc Tribometer

A Pin on Disc (PoD) tribometer is an instrument commonly used to generate and study wear from different types of materials. A common set up consists of a disc and a cylindrical pin, cut out from the real-world materials. The pin is balanced on the disc with a pressure from dead weights on top, as illustrated in Figure 4. As the disc rotates at a selected speed, the friction between pin and disc generates wear particles. By connecting the PoD to particle samplers, such as PM impactors, or other PM measuring instruments, both offline and online analysis can be performed on the generated wear particles (Wahlström et al., 2017).

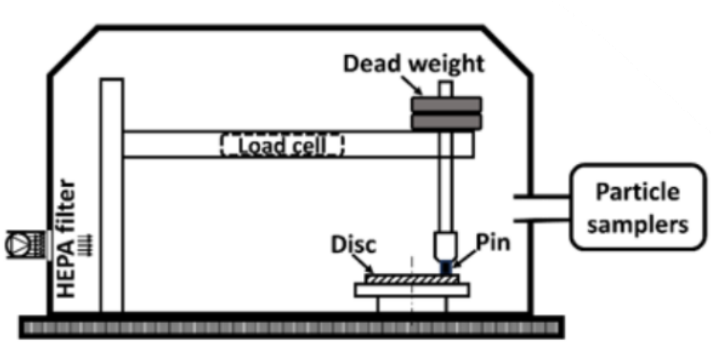


Figure 4: Common Pin on Disc tribometer set up (Lyu et al., 2025)

2.4.2 Particulate Matter measurement instruments

PM_{10} Impactor

A PM_{10} impactor is used to sample aerosols based on particle size. One certain type of impactor is the cascade impactor, where particles are pumped through by an airstream inlet (Dekati, n.d.). The particles are separated and deposited in different stages based on aerodynamic particle diameter (Seville & Wu, 2016). This separation occurs due to the principle of inertial impaction (Salama, 2000). By adding filters to the trays, samples can be transferred and analysed.

Condensation Particle Counter

A condensation particle counter (CPC) is an instrument used to obtain the number concentration of airborne particles. This is achieved by optical counting through light scattering. In order to register particles too small for conventional optical counting, the CPC exposes sampled particles to a supersaturated gas, usually butanol, which then condenses on to the particles. As this occurs, the particle size increases, which enables them to be registered by a laser and counted optically (Kenelec, 2014).

Mini Wide-range Aerosol Spectrometer

A mini wide-range aerosol spectrometer (MiniWRAS) is a combination of an optical particle counter (OPC) and an electrical mobility spectrometer, which allows it to measure both coarse, fine and ultrafine particles. The OPC works by beaming the incoming particles with a laser, causing light to be scattered by the particles. By measuring the amount of scattered light for each particle, an equivalent optical diameter is found and thus classifying the particles by size. Using an assumed density, the particle mass is additionally calculated by the software to obtain PM concentration, which therefore depends on both the measured light scattering and particle density. As a result, the MiniWRAS can produce data for PM_{10}, $PM_{2.5}$ and PM_1 as well as providing particle number concentrations and size distributions (Durag Group, n.d.). However, due to lower sensitivity in the electrometer, the electrical stage in MiniWRAS is usually replaced by a scanning mobility particle sizer (SMPS) to obtain higher accuracy in the nanosized range.

Scanning Mobility Particle Sizer

A scanning mobility particle sizer detects particles through electrical mobility and has high accuracy for nanosized particles. A common set up begins with an initial pre-separator to filter out larger particles which would contaminate the equipment as well as disturbing the measurements. The remaining particles continues into a neutralizer, using a bipolar charger to create a known equilibrium charge distribution over the particles. The charged particles then pass into a differential mobility analyser, where they move through an electric field according to their electrical mobility. Here, the electrical field is systematically scanned for specific electrical mobilities over a certain time interval. The particles with matching mobility are sorted out and introduced into a CPC. Since the electric mobility is a function of charge and size, particle size can be calculated by inversion using an assumed mobility diameter. As a result, the polydisperse aerosol input becomes monodispersed (Brouwer et al., 2014; TSI Inc., 2022a).

2.4.3 Energy Dispersive X-ray Fluorescence Spectrometry

Energy dispersive X-ray fluorescence (EDXRF) analysis is a non-destructive method for analysing the elemental composition of a sample. This is performed by using X-rays to excite electrons within the elements in the sample. The excited electron is ejected from the element, which causes outer electrons to take its place and consequently release excess energy in the form of an X-ray, which is measured by the spectrometer. The energy released differs from each element, and as such, the EDXRF spectrometer can identify and quantify the elements present in the sample (Figure 5) (Rigaku, n.d.). However, EDXRF is limited by the mass of the measured elements. Lighter elements, such as Al and Mg, generally produce X-rays with lower energy and are as such harder to be detect by the machine, and elements with too low density cannot be detected at all, e.g. He and Li. As such, EDXRF is more reliable for measuring elements with higher atomic numbers (Rigaku, 2025).

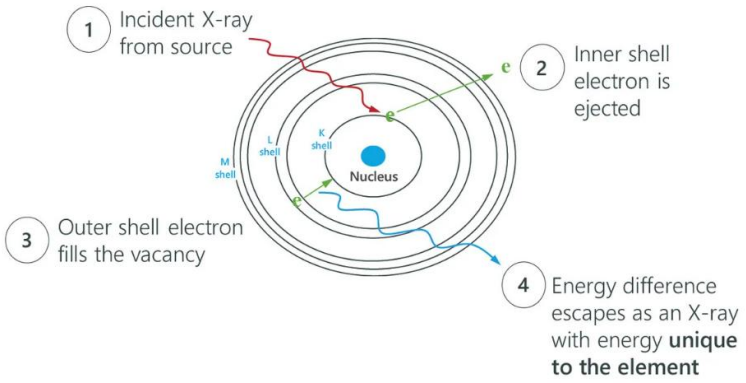


Figure 5: The process of EDXRF analysis (Rigaku, n.d.)

2.4.4 Water Soluble Tetrazolium Assay

The toxic effect of an element or chemical agent can be investigated through cell viability assays. Using living cells, the resulting effect is either cytotoxic or cytostatic, meaning cell death or inhibition of cell growth. One such cell viability assay is the water-soluble tetrazolium assay (WST). The WST-assay is a colorimetric assay, meaning the result is indicated through a change in colour. This is done by reduction of a tetrazolium salt, which produces a colourful formazan compound. The reduction is performed by living cells using mitochondrial dehydrogenase enzymes to break down the formazan. In the test, this is done in the presence of the potential toxic agent. This means that if the tested compound is cytotoxic, the metabolism will decrease and the colouring will be weaker. Since the formazan produced is directly proportional to the amount of active dehydrogenase,

it is a measurement of metabolic activity, and consequently, how the agent affects cell viability. The viability is evaluated by measuring absorbance of the WST reagent, where low absorbance indicates low cell viability. An advantage of using WST instead of other assays is that the procedure is simple and fast, however, the result only indicates cell activity, not cytotoxicity directly (Kamiloglu et al., 2020; Präbst et al., 2017).

2.4.5 Detection of Intracellular Reactive Oxygen Species

A common cellular response to brake wear is the formation of ROS, which cause oxidative stress and have potential cytotoxic effects. Intracellular ROS production can be investigated by using the probing with a chloromethyl derivative of 2', 7' dichlorofluorescein diacetate (CM-H_2DCFDA). When added, CM-H_2DCFDA is taken up by cells though passive diffusion. If the cells are subsequently exposed to a ROS forming substance, CM-H_2DCFDA is oxidized to 2', 7'-dichlorofluorscein (DCF), which is highly fluorescent. This resulting fluorescence can be measured using e.g. a fluorometer or microplate reader. Consequently, higher fluorescence indicates higher ROS production. By measuring fluorescence at different time intervals, including in the very beginning of the exposure, the increased ROS production over time can be determined (Ameziane-El-Hassani & Dupuy, 2013; Molecular Probes, 2006).

3 Materials and design of experiments

To achieve the aim of this project, three types of brake pads were investigated through online and offline experiments. The online analysis was made for airborne particles and was constructed to determine PM_{10} concentration, PNC and particle size distribution. For the offline analysis, two types of particles were collected: non-airborne particles and airborne particles. Both the non-airborne particles and the airborne particles were analysed for elemental composition, while the airborne particles were additionally analysed for cell toxicity. An overview of materials and design of experiments is presented in Table 1.

Table 1: Overview of materials and design of experiments

	Materials	Online tests	Particle collection	Offline tests
Description	Three different brake pads.	PM_{10} - concentration, PNC, size distribution.	Airborne particles collected on water soluble filters. Non-airborne particles collected on teflon filters.	Elemental composition, Cell viability, ROS production
Instruments and experimental methods	-	MiniWRAS, CPC, SMPS	Pin on Disc tribometer, PM_{10} impactor.	EDXRF, WST-1 assay, CM-H_2DCFDA assay

3.1 Materials

The materials used for this project are the same as in the experiments done by Lundin (2024). This includes three types of commercial HDV brake pads, which are referred to as Pad 1, Pad 2, and Pad 3, as well as a rotor disc made of grey cast iron. The brake pads were all semi-metallic and the overall material composition is shown in Table 2. Already used brake pads were tested in order to reduce the bedding in period (Lundin, 2024).

Table 2: Brake pad material composition.

Ingredient	Pad 1 (%)	Pad 2 (%)	Pad 3 (%)
Iron	20 - 35	27 – 36,1	27 - 37
Graphite	5 - 20	7,6 - 11	9 - 14
Calcined petroleum coke	5 - 20	7,6 - 12	17 - 22
Chromite	2.5 - 7.5	3,2 – 5,2	-
Metal oxides	7 - 24	10,5 – 17,5	21 - 31
Metal sulphides	2 - 12	1,2 – 8,4	2 - 5
Other types of metals	8 - 24	10,3 – 14,8	-
Phenol, polymer with formaldehyde	5 - 15	3,6 – 6,15	5 - 8

3.2 Online Analysis

Particles were generated using a NANOVEA® T50 PoD tribometer. The set up is displayed in Figure 6, and consists of a disc, cut out from the disc rotor material, with a diameter of 85 mm and a cylindrical pin with a diameter of 10 mm, cut out from the brake pad material. The tribometer was covered with a plastic hood lined with aluminium foil to prevent particles from attaching to its inside. Inside the hood, a clean air supply through a HEPA-filter was connected, with an air flow of 66 l/min. The dimensions of the tribometer are presented in Table 3, and are based on the dimensions concluded by Lundin (2024). The following online measurements were conducted:

- To measure PM concentration and present size distributions, a GRIMM® MiniWRAS model 1.371 was used. Sampling was done with a metal tube and an aerosol airflow of 1.2 l/min. Measurements in the MiniWRAS was done using only OPC, which optical channels detect particles between 30 and 0.2 µm. For the calculation of PM concentrations, a density of 1 g/cm^3 was assumed. The data from the electrical mobility spectrometer was disregarded (Durag group, n.d.)
- To measure nanosized particles for size distributions, a TSI® SMPS model 3938 was used. Sampling line from the PoD consisted of a Tygon® tube. This was connected to a pre-impactor, filtering out particles with an aerodynamic diameter over 0.8 µm. The aerosol airflow into the SMPS was 0.3 l/min (TSI Inc., 2022a). The time interval for the measurements was three minutes, and the measured size range based on electrical mobility diameter was 18 nm – 1000 nm.
- Particle number concentration was measured with a TSI® CPC model 3752, using a metal line and butanol as condensation gas. The instrument detects particles down to 4 nm (TSI Inc., 2022b).

Measurements were made for three different sliding conditions for each of the three brake pad materials, called low condition, high condition and extreme condition. This was in order to simulate braking at three different velocities: 36 km/h, 62 km/h and 81 km/h. Each condition was repeated two times for each pad material. The test variables for the online measurements are presented in Table 4. The collected data was analysed to present PM_{10} concentrations, PNC, particle size distributions for each pad material and sliding condition.

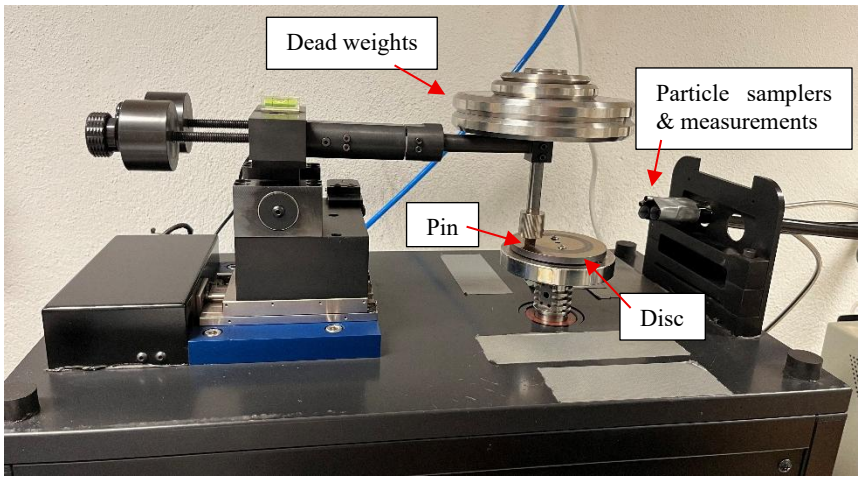


Figure 6: Experimental set up of the PoD tribometer.

Table 3: Dimensions of PoD tribometer

	Pin on Disc	Real HDV
Tire diameter	-	1073 mm
Effective radius (inner)	27 mm	168 mm
Brake disc diameter	85 mm	260,22 mm
Brake pad area	78,54 mm^2	$14*10^3$ mm^2
Pressure	0,6 MPa	-
Weight on pin	47 N	-
Air flow	66 l/min	-

Table 4: Test variables online measurements

Temp.	Setting	rpm	Sliding velocity	Vehicle velocity	Driving pattern	Test duration
195 °C	“Low”	1100	3,11 m/s	36 km/h	Urban driving	1,5 hours
280 °C	“High”	1900	5,37 m/s	62 km/h	Rural driving	40 min
-	“Extreme”	2500	7,07 m/s	81 km/h	Highway driving	25 min

3.3 Collection of particles

Particles collected for offline analysis were generated using the PoD with the same dimensions as the online measurements (Table 3) and a similar set up. The difference was that instead of measurement instruments, a Dekati® PM_{10} impactor was connected through an inductive line. The airflow through the impactor was 30 l/min. The tribometer was run for two different sliding velocities, corresponding to a real HDV driving at 36 km/h and 62 km/h. A complete set up is displayed in Figure 7.

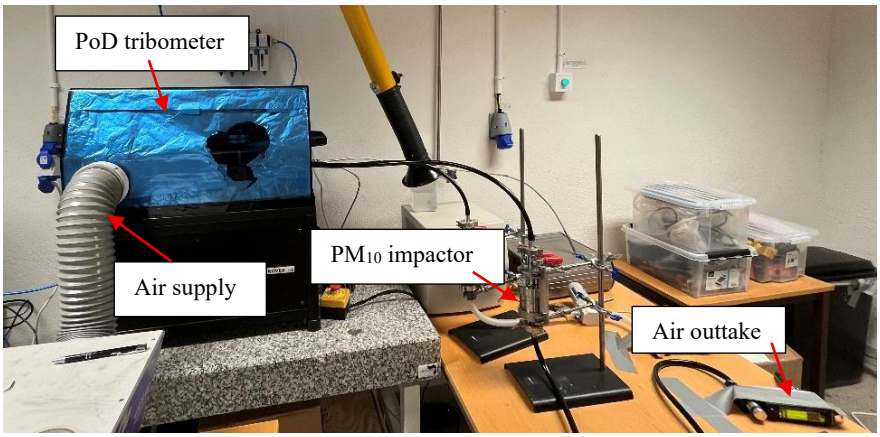


Figure 7: Complete experimental set up of particle collection.

The samples of particles were collected on two different filters, one PTFE teflon filter with pore size 1 µm, and one water-soluble filter made from polyvinyl alcohol. The water-soluble filter is comparable with PTFE and quarts filters in terms of durability and weather resistance (Yang et al., 2026). The teflon filter was taped to the bottom of the tribometer to gather non-airborne, fast settling particles, as illustrated in Figure 8. In the PM_{10} impactor, the water-soluble filter collected airborne particles. Both filters were used for EDXRF analysis, only the water-soluble filter was used for cell toxicity analysis. For each pad tested, particles generated by both low and high sliding velocities were gathered onto the same filter, meaning that each pad tested resulted in two filters, giving six samples in total. Additionally, two blank filters were analysed in order to account for other particles in the measurements. One filter was a transport blank, where ambient particles in the laboratory were collected. The other was a total blank filter, which was taken directly from the filter package.

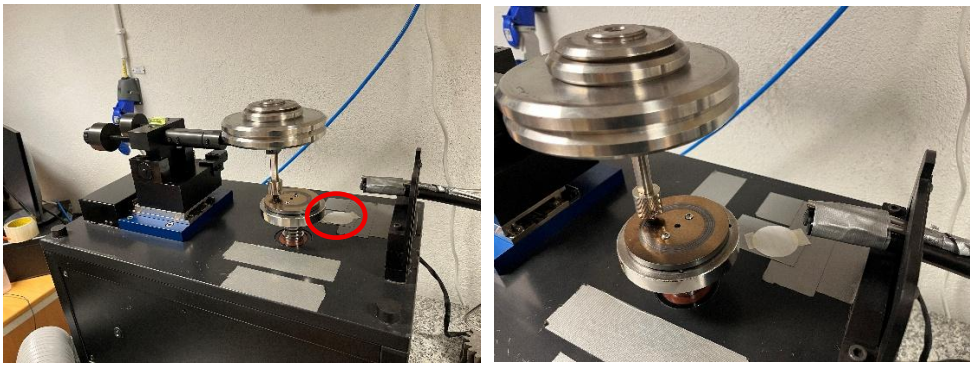


Figure 8: PoD tribometer with taped down teflon filter, collecting non-airborne particles.

In order to obtain enough BWP to carry out the cell viability experiments, it was concluded that the low-velocity tests should run for six hours in total and the high-velocity tests for about five hours. This was calculated using the previous findings of Lundin (2024), test runs and the mechanical relationships are presented in Appendix A. Due to high temperatures developed during the test, the low-velocity test was run in two intervals of three hours and the high-velocity test in eight intervals of 40 minutes, with at least 30 minutes of cooling time in between (Table 5).

Table 5: Running schedule for particle collection at the different settings

Test setting	Running time	Intervals	Cooling time
Low	3 h	2	1 h
High	40 min	8	30 min

3.4 Offline analysis

3.4.1 Particle elemental composition

The elemental composition of the BWP was identified by EDXRF analysis for all six samples as well as the two blank filters. This was carried out using a Rigaku® EDXL-300 spectrometer. Two measurements were made in total, one for the airborne particle samples and one for the non-airborne. To minimize measurements errors, the two blank filters were included at both measurements. Additionally included in both measurements were two standard reference material filters, SRM

2783, which was used to calibrate the EDXRF spectrometer and ensure measurement accuracy.



Figure 9: EDXRF preparation.

3.4.2 Cell exposure tests

The conducted cell exposure tests were the WST-1 assay and ROS detection assay with CM-H2DCFDA probing. Both procedures were performed using brake dust exposure suspensions, prepared prior to the tests (Figure 10). To calculate the dose of BWP for the suspensions, the total particle mass collected on the water-soluble filters was calculated. This was done as an approximation of the element mass presented in the EDXRF analysis. The results from the EDXRF could be used to calculate the combined mass of all measured elements per cm^2. The total mass was found by assuming a filter area equal to 16 cm^2. This approximation was done as an alternative solution to not being able to use a semi micro balance, due to the water filter absorbing moisture thus overestimating the weight of the particles.

The brake wear suspensions were prepared by cutting 1/8 of the sample filter and dissolving it in Minimum Essential Medium (MEM). One suspension for each pad, as well as the transport blank filter, was made. The amount of MEM was adjusted to give a particle concentration of 500 µg/ml per suspension tube. The added MEM for the transport blank suspension was 2.21 ml, the rest of the volumes are presented in Figure 10. A TOMY® Ultrasonic disruptor UD-100 was used to fully dissolve the samples. Lastly, the samples were further diluted in with MEM in a series of four particle suspensions for each filter with concentrations of 100, 50, 25 and 12.5 µg particles/ml respectively, giving 16 particle suspensions in total.

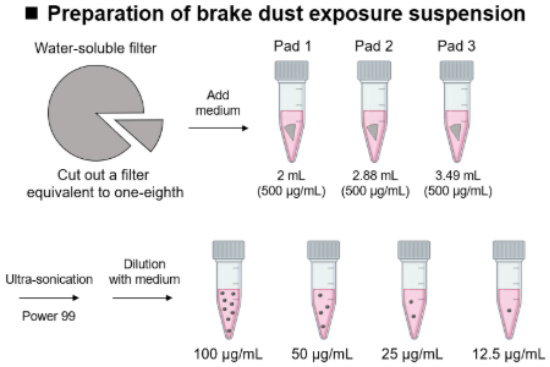


Figure 10: Schematic display of preparation of brake dust exposure suspensions and the added amount of MEM. A fourth suspension for the blank transport filter was additionally made with 2.21 ml E-MEM (Raga Ishikawa, Keio University)

3.4.2.1 WST-1 assay, cell viability

Cell viability was investigated using the WST-1 assay. The procedure is illustrated in Figure 11, and was initiated by suspending priorly cultivated human epithelial A549 lung cells with E-Minimum Essential Medium (E-MEM) to a concentration of $6.13*10^6$ cells/ml. From this suspension, 100 µl was seeded on a 96-well plate, resulting in a concentration of 10^4 cells/well. In total, two 96-well plates were prepared and incubated for 24h.

Subsequently, the brake dust exposure suspensions were prepared as described, using E-MEM. Before the exposure, the prepared cells were washed with Phosphate-Buffered Saline two times to remove eventual residual E-MEM, which otherwise would interfere with the absorbance measurements. After this, the exposure was performed by adding 100 µl of each of the previously prepared brake dust exposure suspensions to the incubated plates. The suspensions were added both to the already cell-containing wells, and to additionally previously empty wells. These blank empty wells were needed to calibrate for the absorbance of the medium. Lastly, one column of wells was left without brake dust suspension, to serve as control. A theoretical illustration of the resulting plate after the test is shown in Figure 12.

After 24h incubation, pink WST-1 reagent was added to all 72 wells. Absorbance was measured after 30 min incubation using a AS ONE® MPR-A100 microplate reader. The relative cell viability was calculated by subtracting the average absorbance of the pink blank empty wells from each corresponding sample well and then dividing with the control average (Appendix D.1).

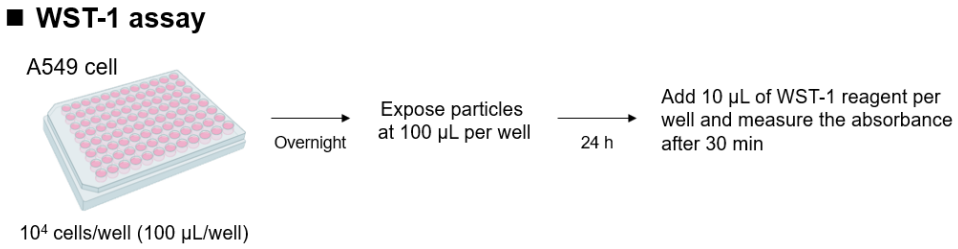


Figure 11: Illustration of the WST-1 assay procedure (Raga Ishikawa, Keio University)

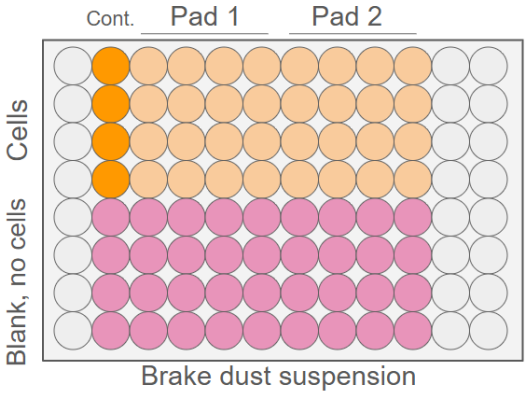


Figure 12: Illustration of a theoretical resulting plate in the WST-1 assay. Orange wells contain cells, pink wells do not. All coloured wells contain brake dust suspension, except the second column to the left (marked Cont.) which serves as control (Olga Schubert)

3.4.2.2 CM-H_2DCFDA, ROS detection assay

The production of reactive oxygen species was tested using CM-H_2DCFDA probing. The process is illustrated in Figure 13. The tested cells were priorly cultivated human epithelial A549 lung cells, which was suspended in Minimum Essential Media Alpha (MEM-alpha). From this suspension, 100 µl was added to the wells on a96-well plate, resulting in a concentration of $2*10^4$ cells/well. A black plate was used to be able to measure the resulting fluorescence. In total, one 96-well plate was prepared and incubated for 24h.

Before cell exposure, the ROS-probe was prepared by dissolving CM-H_2DCFDA in dimethyl sulfoxide, obtaining a concentration of 5 µM/l. A volume of 100 µl was added to each well. Additionally, the cell plates were prepared by washing with phosphate-buffered saline to remove residual MEM-alpha which could disturb the fluorescence measurements. Brake dust exposure suspensions were prepared in the same way as for the WST-1 assay, with the difference of using MEM-alpha instead of E-MEM.

The cells were exposed by adding 100 µl from each of the prepared particle suspensions to the cell containing wells except for one column to be used as control. After exposure, fluorescence was measured at different time intervals, using a TECANO® INFINATE F NANO microplate reader. Fluorescence was measured initially, at 0h, then again after incubation for 1h, 3h, 6h and 24h. The relative ROS-production was calculated by dividing every sample measurement with the initial measurement at time zero (Appendix D.2).

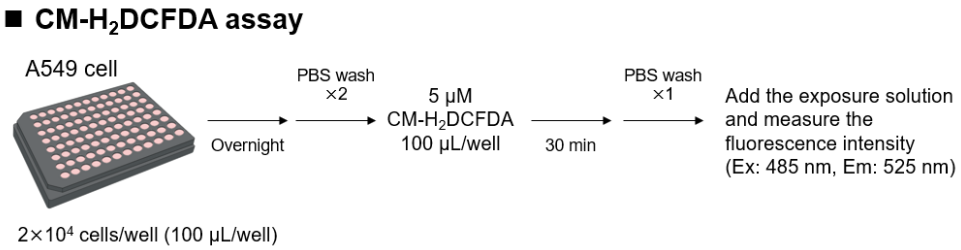


Figure 13: Illustration of ROS detection assay procedure, using CM-H2DCFDA (Raga Ishikawa, Keio University)

4 Results and discussion

This section is dedicated to presenting the results from all performed experiments and discuss their interpretation. This includes online PM measurements as well as offline results from particle collection, EDXRF-analysis and cell exposure tests.

4.1 Particle collection

The resulting six filters with BWP collected from each pad, both airborne and non-airborne particles are displayed in Figure 14. This is the result of particle collection according to Table 5. By calculating the mass of the water-soluble filter, it is concluded that Pad 3 generated the largest particle mass, followed by Pad 2 and lastly Pad 1 (Table 6).

Moreover, the mass of the collected non-airborne particles was not examined during this study. This is due to uncertainties of loose particles as there was no airflow through the filter. To draw conclusions of the non-airborne particles based only on the sample's visual appearance, would be incorrect.

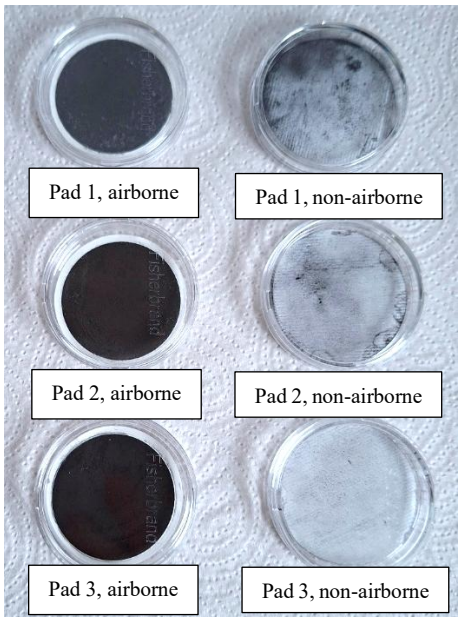


Figure 14: Samples of collected airborne and non-airborne BWP for Pad 1, 2 and 3.

Table 6: Particle mass of airborne particles collected on the water-soluble filter.

Pad	Weight airborne particles (mg)
1	8.05
2	11.52
3	13.94

4.2 Online analyses of particulate matter

In the following subsections, the results of the online measurements of PM_{10}, PNC and size distribution are presented. The data for all parameters will be presented as an average between the two runs for the same setting for each pad material. The pads will, in the following figures, be referred to as P1, P2 and P3 which correspond to Pad 1, Pad 2 and Pad 3.

To accurately depict each material's properties, the bedding period has been removed from the results. For PM_{10} concentrations and PNC this entails exclusion of roughly 15 minutes of data since the start of the experiment at low (1100 rpm) and high (1900 rpm) settings. Due to a shorter running time of the extreme setting (2500 rpm) the corresponding excluded time is about 10 minutes. Graphs including all repetitions are shown in Appendix B. Similarly, the results of the size distribution were averaged for a span of 18 minutes for the low and high settings, and 15 minutes for the extreme setting.

4.2.1 PM_{10} concentration

The PM_{10} measurement results for the various pads and condition settings are shown in Figure 15 - Figure 17. The results are formatted as averages between two runs during steady state, whilst the figures with both runs are illustrated in Appendix B1.1. As can be seen in Figure 15 - Figure 17, the PM_{10} concentration generally increases with higher sliding condition, regardless of material, which could be explained by increased wear through thermal degradation and tribo-oxidation. To clarify the differences in results between the different settings, the averages of both individual runs and the averages between the two during steady state are presented in Table 7. Additionally, Figure 15 - Figure 17 as well as Table 7 show that Pad 3 generates the highest PM_{10} concentration, followed by Pad 2, while Pad 1 is constantly lower, regardless of sliding condition. The results thus indicate that there

is a clear difference in generation of PM_{10} concentration depending on the material chosen even if all increase at a higher sliding velocity.

However, the absolute PM concentration might be underestimated. According to Woo et al. (2021), OPC usually presents three times lower PM values when measuring BWP, compared to gravimetric studies. To examine this, new PM_{10} concentrations was calculated from the obtained particle mass shown in Table 6 (Appendix B 1.2). This resulted in average PM_{10} concentrations of 395 $\mu g/m^3$, 565 $\mu g/m^3$, 683 $\mu g/m^3$ for Pad 1, 2 and 3. When comparing these results with Table 6, one can see that the calculated concentrations far exceed the ones measured. Nonetheless, the measurements still serve its purpose of this study as intended, which is as a comparison between three sample types. The old data obtained by Lundin (2024) with the same materials and similar settings are also shown in Table 7. It can be seen that the current study achieved highly comparable results with Lundin's, indicating that the method used in the current study is reliable and repeatable. Note that Lundin's study didn't have the extreme setting as in the current study.

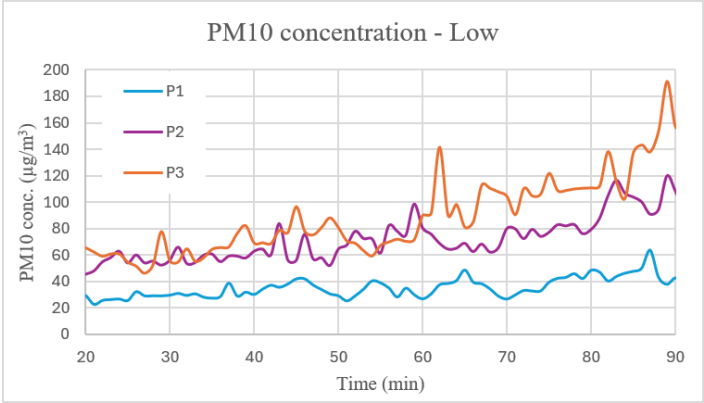


Figure 15: PM_{10} concentration for each pad at low condition (1100 rpm).

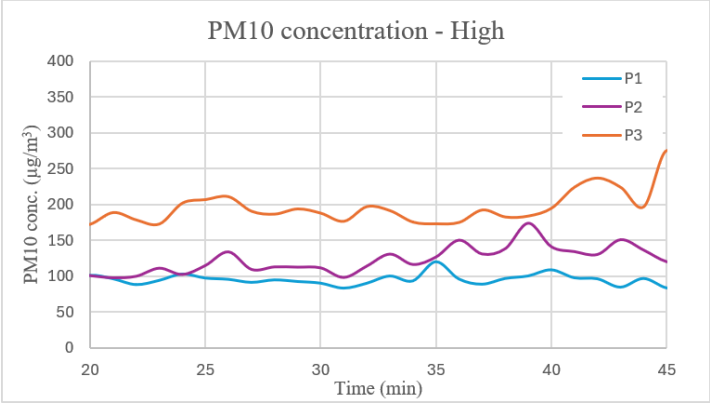


Figure 16: PM_{10} concentration for each pad at high condition (1900 rpm).

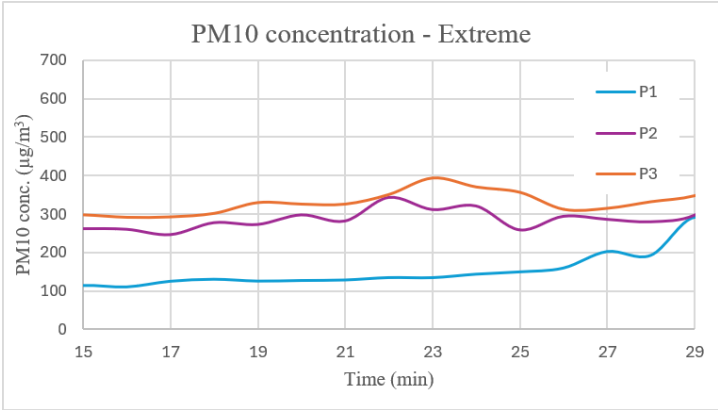


Figure 17: PM_{10} concentration for each pad at extreme condition (2500 rpm).

Table 7: Averages of PM_{10} and $PM_{2.5}$ for each repetition over the same timespan as presented in Figure 15 - Figure 17

Pad nbr	Settting	Run	This study			J. Lundin (2024)
			PM2.5 /PM10 (%)	PM2.5 (µg/m^3)	PM10 (µg/m^3)	PM10 (µg/m^3)
Pad 1	Low	L1	52	14,04	27,20	26,22
		L2	47	20,39	43,44	34,44
		L3				37,31
		Avg L	49	17,22	35,32	32,66
	High	H1	45	30,15	67,17	107,44
		H2	43	52,27	121,33	111,48
		H3				124,83
		Avg H	44	41,21	94,25	114,58
	Extreme	E1	58	92,99	160,13	
		E2	46	55,55	121,71	
		Avg E	53	74,27	140,92	
Pad 2	Low	L1	50	30,49	61,05	75,01
		L2	46	39,01	84,10	72,18
		L3				224,53
		Avg L	48	34,75	72,57	123,91
	High	H1	53	58,50	109,83	120,21
		H2	50	67,99	137,27	169,02
		H3				
		Avg H	51	63,24	123,55	144,61
	Extreme	E1	51	153,94	300,23	
		E2	49	139,93	288,31	
		Avg E	50	146,94	294,27	
Pad 3	Low	L1	48	35,31	73,74	41,85
		L2	49	51,72	106,35	58,48
		L3				56,06
		Avg L	48	43,52	90,04	52,13
	High	H1	45	97,62	214,88	105,96
		H2	47	83,98	179,63	148,57
		H3				99,29
		Avg H	46	90,80	197,26	117,94
	Extreme	E1	45	140,98	315,08	
		E2	40	143,57	355,94	
		Avg E	42	142,27	335,51	

4.2.2 Particle number concentration

The results from PNC measurements for the various pads and condition settings can be seen in Figure 18-Figure 20. The results are formatted as averages between two runs during steady state, whilst the figures with both runs are illustrated in Appendix B2. The results show that Pad 1 consistently generates the lowest PNC regardless of setting, followed by Pad 2 and lastly Pad 3. However, as seen in Figure 18 the difference between Pads 2 and 3 at 2500 rpm is a bit diffuse as the fluctuations in PNC makes the order harder to decipher. To clarify, the averages of both individual

runs and the averages between the two during steady state are presented in Table 8. Lundin's (2024) old data is also shown in the table for comparison and repeatability evaluation. Although one of the repetitions for Pad 2 exceeds the average PNC for Pad 3, the total average for both pads show that Pad 3 produces the highest PNC. As follows, these results can be summarised as Pad 1 generating the lowest PNC followed by Pad 2 and lastly Pad 3, which generates the highest, even though the difference between the latter two is less certain.

Seemingly, the PNC changes as sliding velocity and temperature increases. When observing Figure 18 - Figure 20 as well as Table 8, it can be noted that the PNC consistently increases with a higher setting for each pad. The origin of this increase in PNC might be because of additional particle generation by thermal degradation, possibly creating more ultrafine particles compared to what is generated with mechanical abrasion. Since the extreme setting generates higher temperatures, this is a plausible explanation for the increased PNC shown in Figure 20. Consequently, PNC seems to increase with sliding velocity and temperature.

Moreover, there seems to be a difference in stability between the materials. As observed in Figure 18 - Figure 20, Pad 1 shows the least fluctuations during the test runs, while this is not true for Pad 2 or Pad 3. Most noticeable are the spikes produced by Pad 3 in Figure 18. A plausible reason for these spikes is repeated formation and destruction of secondary plateaus in the brake pad material. Secondary plateaus are created when dislodged BWP adhere to the reinforcing fibres of the primary plateaus. Eventually there will be a change in the contact situation, causing the secondary plateaus to break off and be grinded down once again into wear particles (Wahlström, 2011). As this occurs, a larger number of particles are released into the surrounding areas in one occurrence, seen as a spike of PNC in online measurements, or new secondary plateaus are formed. The reason why Pad 3 is more prone to have such spikes is likely due to its material properties, which will be discussed in section 5. Why these spikes are particularly present in the lower setting (Figure 18) is likely due not due to sliding velocity or temperature, but rather that the longer running time which allowed this repeated formation and destruction of plateaus to be showcased. As shown in Figure 18 to Figure 20 the materials differ in stability, with Pad 1 continuously producing stable levels of PNC, unlike Pads 2 and 3.

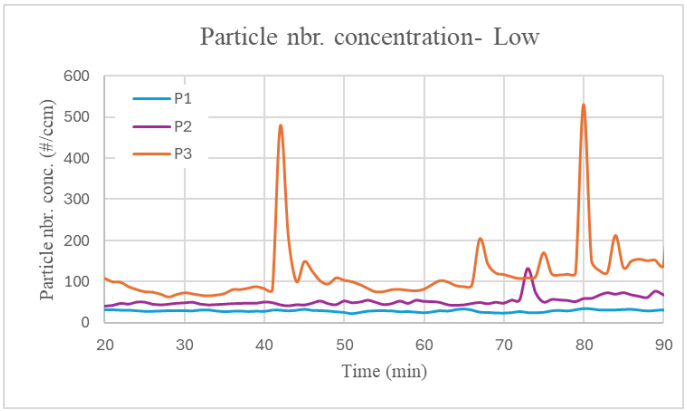


Figure 18: Particle number concentration for each pad at low condition (1100 rpm).

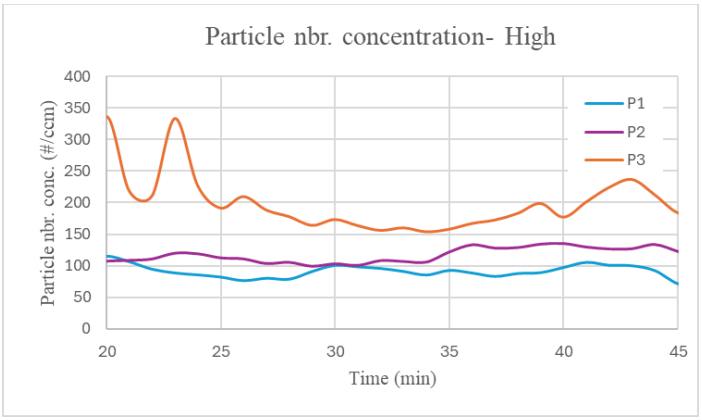


Figure 19: Particle number concentration for each pad at high condition (1900 rpm).

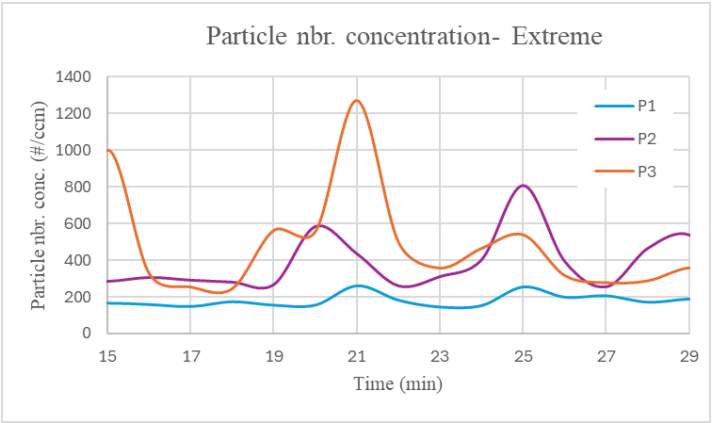


Figure 20: Particle number concentration for each pad at extreme condition (2500 rpm).

Table 8: PNC averages from each repetitionTable 8: PNC averages from each repetition over the same timespan as presented in Figure 18 - Figure 20.

Pad nbr	Settting	Run	This study	J. Lundin (2024)
			PNC (#/ccm)	PNC (#/ccm)
Pad 1	Low	L1	27,89	15,43
		L2	30,51	76,04
		L3		23,76
		Avg L	29,20	38,41
	High	H1	71,91	130,17
		H2	108,26	104,49
		H3		360,53
		Avg H	90,08	198,40
	Extreme	E1	232,15	
		E2	134,05	
		Avg E	183,10	
Pad 2	Low	L1	53,97	42,75
		L2	54,08	31,89
		L3		164,36
		Avg L	54,02	79,66
	High	H1	115,36	109,03
		H2	119,44	140,77
		H3		
		Avg H	117,40	124,90
	Extreme	E1	472,41	
		E2	316,00	
		Avg E	394,21	
Pad 3	Low	L1	109,97	55,48
		L2	131,00	42,39
		L3		67,40
		Avg L	120,48	55,09
	High	H1	199,45	118,35
		H2	188,56	225,23
		H3		113,51
		Avg H	194,00	152,37
	Extreme	E1	421,16	
		E2	465,04	
		Avg E	443,10	

4.2.3 Particle size distribution

Size distributions are presented in Figure 21 - Figure 23, combining data measurements from the optical channels in the MiniWRAS with the data from SMPS. The results are formatted as averages between two runs during steady state, whilst figures with both runs are illustrated in Appendix B.3. It should be noted that MiniWRAS measures particle size by an equivalent optical diameter and the SMPS by a mobility diameter. The size distribution is number weighted in order to not underestimate potential UFP. As can be seen, the main size range of the particles is between 200-1000 nm, for all three pads and all three conditions. Some UFP can be

observed, but at very low concentrations. Consequently, the dominating number particle fraction is $PM_{2.5}$.

The results of the size distribution show little variation and are quite consistent regardless of pad or sliding condition. The mode size for all materials is about 400-500 nm in diameter. Since this a number-weighted distribution, it is more sensitive for smaller particles which results in a distribution more shifted to the left compared to a mass weighted distribution. This size mode has been found in previous study (Lyu et al., 2024). However, as literature points out, the number of fine and ultrafine particles usually increase with higher temperature, due to increased thermal degradation, but is not observed in the current study.

In addition to the number weighted size distribution results, the fraction of $PM_{2.5}$ within the total PM_{10} (Table 7). This analysis shows that, for each pad BWP, about half of the mass of PM_{10} concentration lies in the $PM_{2.5}$ fraction. This is higher compared to the general findings in the literature, which concludes that $PM_{2.5}$ to be mainly about 30-40% of the total airborne BWP, however, the share found in this study has been observed before (Lyu et al., 2024).

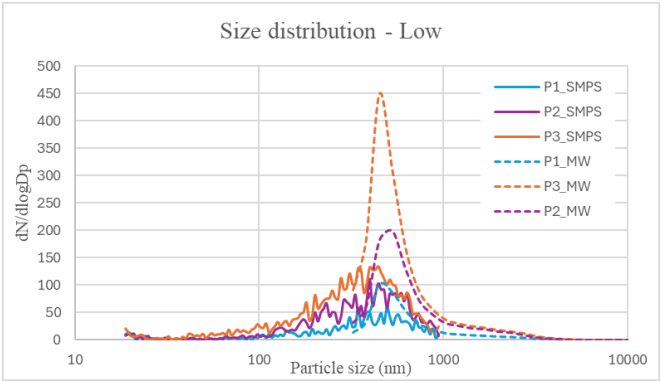


Figure 21: Particle size distribution for each pad material at low condition (1100 rpm). SMPS is presented using the mobility diameter and MiniWRAS the optical diameter respectively.

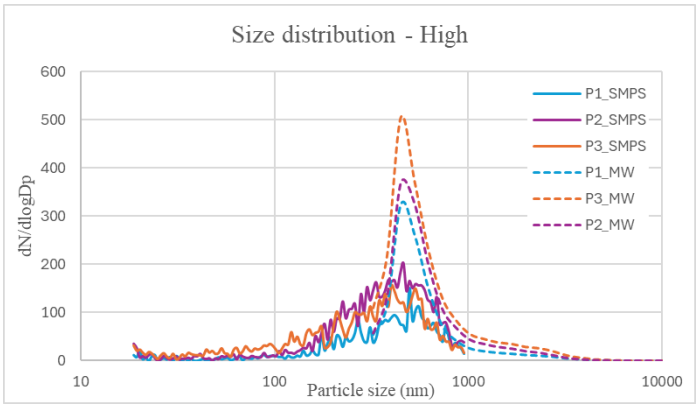


Figure 22: Particle size distribution for each pad material at high condition (1900 rpm). SMPS is presented using the mobility diameter and MiniWRAS the optical diameter respectively.

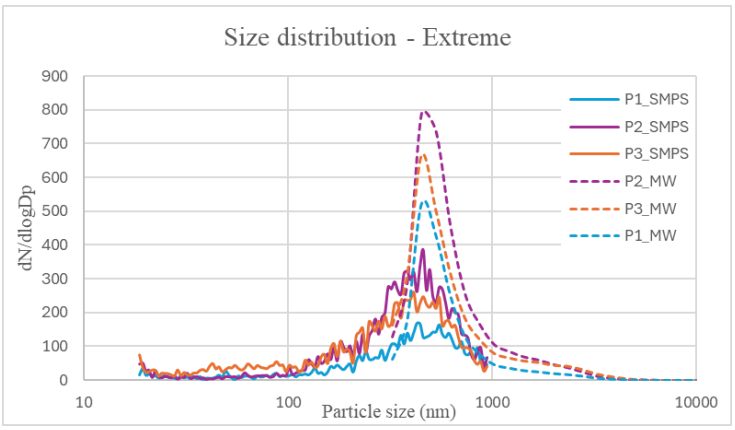


Figure 23: Particle size distribution for each pad material at extreme condition (2500 rpm). SMPS is presented using the mobility diameter and MiniWRAS the optical diameter respectively.

4.2.4 General discussion online measurements

To summarize, there are clear differences in emission patterns for the different brake pad materials which are consistent throughout the different measurement results. Evaluating both PM_{10} concentrations and PNC, it can be observed that Pad 3 produced the highest BWP emissions followed by Pad 2 and lastly Pad 1 (Figure 15 – Figure 20). This becomes even more clear when the average concentrations are examined (Table 7 and Table 8). In addition, the PM_{10} results further align with PNC by showing a general increase in concentration for all pads with higher sliding velocity. Consequently, the combined results show that Pad 1 generated the lowest

emissions and Pad 3 the highest as well as increased emissions with higher condition setting.

These results support in general the findings of Lundin (2024), who conducted the same online study with the same pad materials, but for only the two lower sliding velocities. The main differences are instead that Pad 2 had the highest BWP emissions, both regarding PM concentration and PNC. However, this can be explained by the limited number of repetitions performed for each material. As described by Lundin (2024), this highlights the issue of greater variations between runs, possibly due to inhomogeneous mixing of pad materials.

Furthermore, the results indicate some UPF formation. This is mainly due to the spikes seen in PNC results (Figure 18 – Figure 20). Since similar increase in concentration is not noticeable in the PM_{10} results (Figure 15 - Figure 17), this suggests short and rapid increases of particles within the ultrafine fraction. To investigate this, the size distribution over three spikes was examined. Overall, the investigation found the extracted size distribution to be similar as the ones presented in Figure 21 – Figure 23 i.e. with no clear UFP formation. However, in one case the share of finer particles was higher than the average for that pad and sliding velocity (Appendix B.3.2). Whether this also applies for other spikes cannot be determined, as the SMPS measurement reading time may be too long to capture the short and rapid UFP increase. As a result, an increase in UFP in the PNC spikes can neither be neglected or confirmed.

Overall, the size distribution did not change noticeably with the higher settings. This is somewhat surprising, since thermal degradation is found generally generating particles in the finer fractions, compared to mechanical abrasion. One could therefore expect the size distribution to show an increase in ultrafine particles as the temperature increases, in theory reaching a transition temperature. A small incline with higher temperature in the size distribution can be observed at 10 nm (Figure 21- Figure 23) however, the main mode does not move significantly and since the size distribution is number weighted, such increase in UFP would be more noticeable. Additionally, increasing UFP results in an overall greater increase of PNC compared to PM_{10}, which is not the case for the current study except for the spikes (Figure 15 - Figure 20; Table 7 and Table 8). As a results, this indicates that a higher sliding velocity increases the particle emission concentration but has no substantial effect of particle size.

In contrast to this, a recent and similar study from KTH found significant formation of UFP (Couval et al., 2026). By testing different HDV brake pads, they identified a transition temperature of 150 to 230 °C, at which the PNC greatly increased as a result of increasing primarily UFP. However, it is worth noting that UFP made up the majority of PNC even before the transition temperature. Such transition temperature cannot be observed in this study, even though the lowest temperature is 195 °C. The reason for these differences, despite similar methodology, may be caused by Couval et al. (2026) using new brake pads. The initial run-in period may

affect UFP formation as the material properties is more accurately depicted first afterward. To summarize, the brake material and surface condition might impact the formation of UFP as well as the transition temperature.

4.3 Offline Measurements

4.3.1 Particle elemental composition

The EDXRF results for airborne BWP is shown in Figure 24, and the results from the non-airborne ones in Figure 25. Noticeably, the metal fraction is dominated by iron, exceeding 50% in all brake particles. A large part of iron contribution likely originated from the cast iron disc used in the experiment. Because of this, data is presented both with and without iron to be able to distinguish further differences in the pad material contribution. Some metals with very low concentrations have been excluded from the figures to improve the visibility. The complete data set with all measured elements is presented in Appendix C.1 and C.2.

For the airborne measurements, most iron is found in Pad 3 and the least in Pad 2, reaching 74 % and 58.5 % respectively. Excluding iron from the airborne samples, the rest of the most abundant metals vary between samples. For Pad 1, the second most present metal is 13.82% Cu followed by 3.7% Ca and 3.6% Al. Similarly, Pad 2 also has a high Cu concentration, 9.2%, however Zn and Al have larger shares with 12% respectively 10.7%. In contrast, Pad 3 has a lower Cu content, 0.76%, but contains more Al and Cr, 8.7% and 6.3%.

Similar to the airborne samples, the non-airborne result presents Cu as the most abundant metal after iron in Pad 1, 16.7%, and Zn in Pad 2, 14.8%. For Pad 3, Cr surpasses Al as the most abundant metal (Figure 25). However, all pad materials contain a lower amount of Al as well as a higher amount of Fe compared to the airborne samples. Additionally, the amount of Pb increases from 0.04% to 0.2% in Pad 2 and from 0.04% to 0.12% in Pad 3. A summary of the main differences between airborne and non-airborne samples are presented in Table 9.

In general, elements with lighter densities decrease e.g. Mg and Al, while high-density elements increase marginally, such as Fe, Cu and Pb. As such, the Fe concentration remains the most prevalent for all samples. However, the share of Cu in the non-airborne Pad 3 sample is marginally lower compared to the airborne sample. To summarize, the results of Pad 1 show no change in the most abundant elements, while Al is heavily reduced in the non-airborne sample compared to the airborne one for Pad 2 and Pad 3. Consequently, the lighter element seems to be more prone to become airborne, while the share of heavier elements is similar in both airborne and non-airborne.

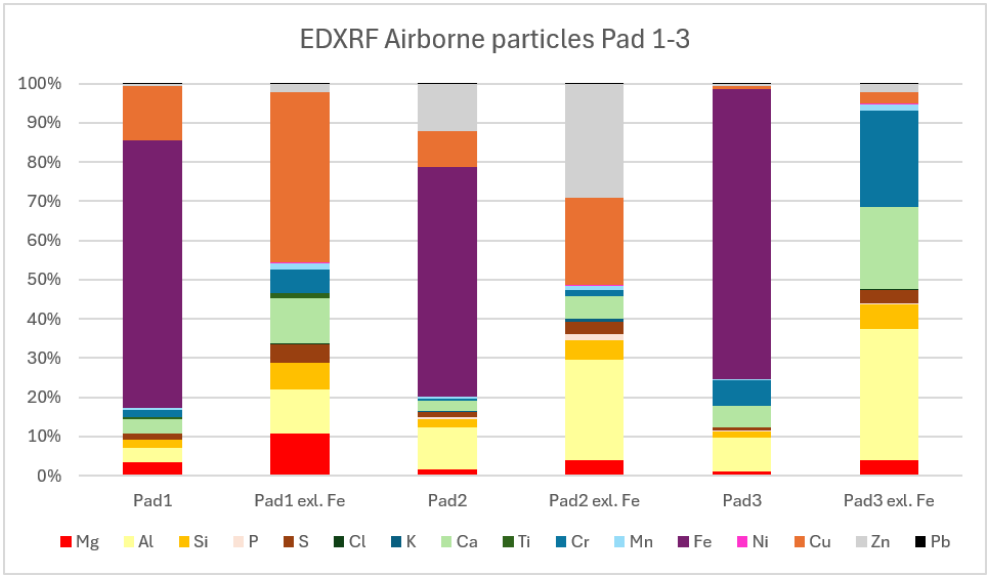


Figure 24: Elemental composition of Pad 1-3 on the airborne particles on the water-soluble filter, both with and without Fe.

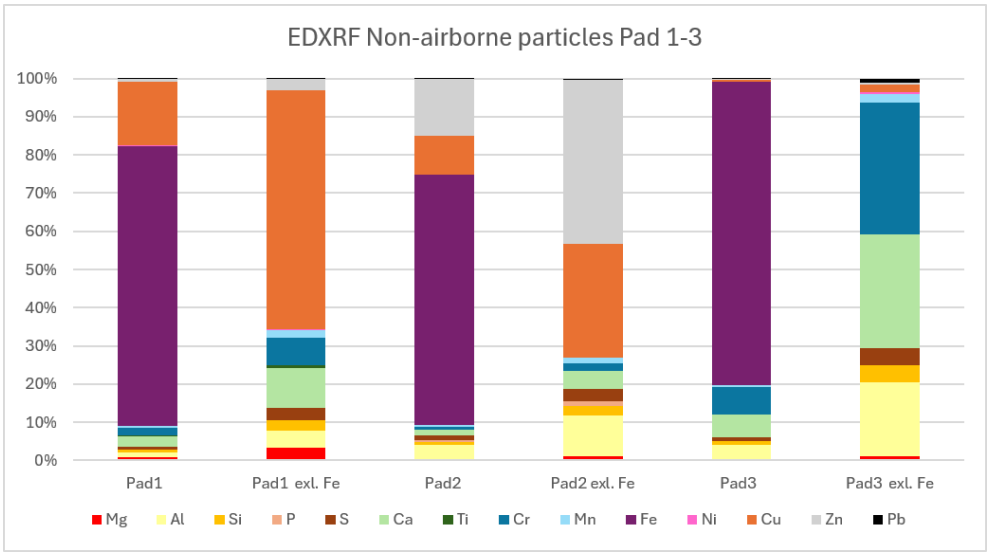


Figure 25: Elemental composition of Pad 1-3 on the non-airborne particles on the teflon filter, both with and without Fe.

Table 9: Total mass concentration of metals, as well as most abundant metals for each pad type. Red: highest fraction, Orange: 2nd highest fraction, Yellow: 3rd highest fraction

		Total concentration ($\mu g/cm^2$)	Percentage of element					
			Fe	Cu	Ca	Al	Zn	Cr
Pad 1	Airborne	503,297	68,2	13,8	3,7	3,6	0,7	2,0
	Non-airborne	n/a	73,2	16,7	2,7	1,2	0,76	1,9
Pad 2	Airborne	720,122	58,5	9,2	2,4	10,7	12,0	0,7
	Non-airborne	n/a	65,6	10,2	1,6	3,6	14,8	0,7
Pad 3	Airborne	871,344	73,9	0,76	5,5	8,7	0,5	6,3
	Non-Airborne	n/a	79,5	0,4	6,1	4,0	0,1	7,1

4.3.2 Cell toxicity

The following two sections are presenting results from the WST-1 assay and the ROS production assay. These tests were conducted with four repetitions for each pad and concentration. However, due to the results of the outer wells being compromised by the surroundings, this number was reduced to n=3, to remove outliers. The complete results are found in Appendix D.1 and D.2.

4.3.2.1 WST-1 assay

The resulting plates from the completed WST-1 assay is displayed in Figure 26, and its data analysis in Figure 27. By visual evaluation of the plates, the orange colour is the most intense in the control column to the left, as well as the first column for each pad, and weakens in the wells to the right where the BWP concentration is higher. Since a weaker colouring indicates less cell viability, this result aligns with a concentration dependent relationship. The weakest colouring is observed for Pad 1, followed by Pad 2 and lastly Pad 3.



Figure 26: Cell viability results. Wells with cells exposed to BWP and WST agent. Orange colouring indicates higher cell viability. Area in black and white is not relevant for this thesis.

The visual evaluation is supported by the data analysis, displayed in Figure 27. In these graphs, the relation between relative cell viability and BWP concentration is presented for each pad material. In addition, the analysis illustrates significance between the different concentrations with asterisk markings. The results showed significant differences between the samples. As seen in Figure 27, Pad 1 and Pad 2 both exhibit a strong dependence of cell viability on BWP concentration. However, the decrease in cell viability for Pad 1 shows a higher significance compared to Pad 2. Regarding Pad 3, one can see that the correlation between the dilution of the sample and the cell viability is less pronounced, indicating a less toxic sample.

However, there is a possibility of overestimating the cell viability decrease for Pad 1. This is due to the wells with BWP from Pad 1 was the first to receive the WST-1 reagent, consequently giving them a longer time to react compared to the wells for Pad 2. Nonetheless, this would not affect the significance of the decrease, which indicates that BWP from Pad 1 still has the most negative effects, regardless of possible overestimation.

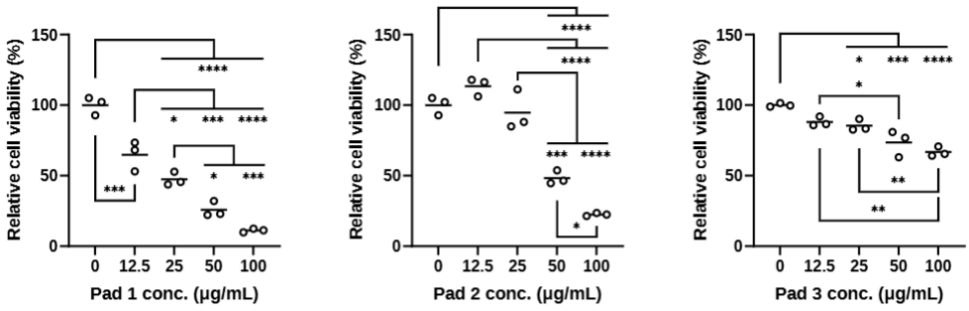


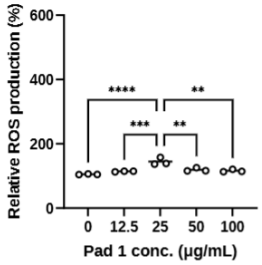
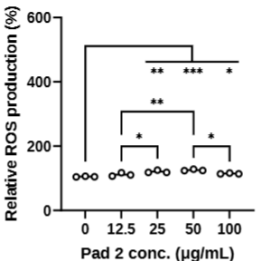
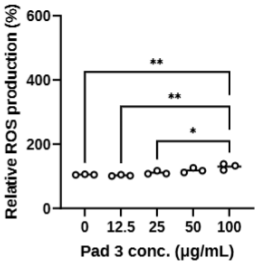
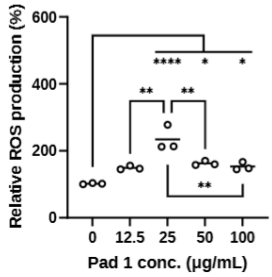
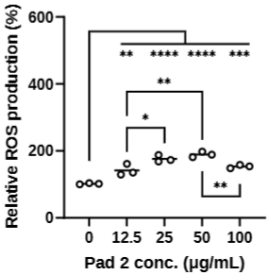
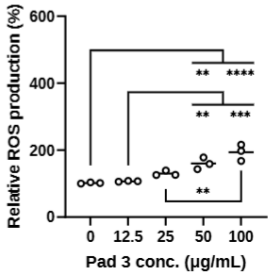
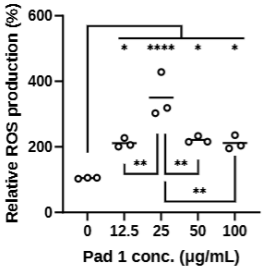
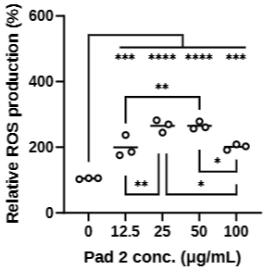
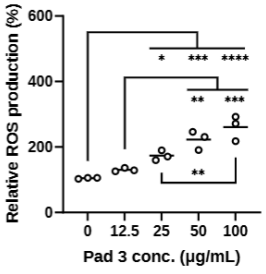
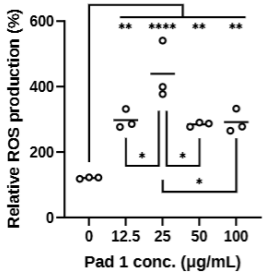
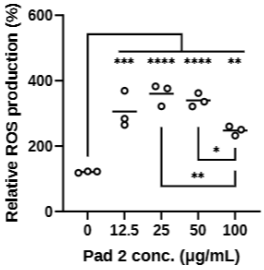
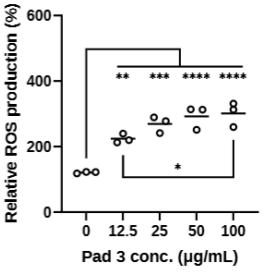
Figure 27: Cell viability results for each pad. Asterisks are marking the significance between the dilution samples, where a higher number of stars indicates a higher significance.

4.3.2.2 ROS detection assay

The relation between relative ROS production and BWP concentration, over time, is presented in Table 10. Similarly to the WST-1 assay, these graphs also illustrate the significance between the different dilution samples but unlike the WST-1 assay, the results from the ROS detection assay allows for repeated measurements. Hence, the results of relative ROS production are presented at 1, 3, 6 and 24 hours.

As shown, the relative ROS production for each pad sample and every dilution concentration increases over time. By comparing the different sample results, Pad 1 and Pad 2 shows similar trends in ROS-production, with higher production for dilution sample 12.5, 25 and 50 µg/ml than for 100 µm/ml. One possible explanation is Pad 1 and Pad 2 have other toxic properties than ROS production. If this is the case, a higher concentration of BWP from these pads might have cytotoxic or cytostatic effects before the ROS production can increase in these suspensions. In contrast, Pad 3 shows a more linear relationship between ROS-production and BWP concentration, indicating weaker ROS inducing capacity of the particles.

Table 10: ROS-production results at hour 0, 1, 3, 6, 24, for each pad. Asterisks are marking significance between dilution samples, with a higher number of stars indicating higher significance.

	Pad 1	Pad 2	Pad 3
1h			
3h			
6h			
24h			

4.3.3 General discussion offline measurements

The offline measurements showed that BWP from all three pad materials caused decreasing cell viability. Thus, it indicates that all pads have cytostatic or cytotoxic effects. It should be noted that the cell viability test does not show the toxicity itself, only a decrease in cell function, however, this is still an indication of negative effects from the BWP.

The cause of these effects is linked to the EDXRF results, which present that all pads contain elements with intrinsic toxic properties such as the heavy metals Fe, Cu, Zn, Pb as well as the lighter metal Al. These results were expected, since all these are common elements found in both the BWP and the different materials used in brake pads. Fe is the most abundant of these metals; however, whether it originates from the pad or the disc cannot be clearly distinguished. The particle collection containing the most Fe was from Pad 3, which also had the weakest decreasing cell viability. Therefore, Fe is not the dominant element causing the negative effects on the cells.

Instead, the decreasing cell viability is likely due to Cu. This is attributed to the strongest decrease found in the particle collection from Pad 1 and Pad 2, which also had higher Cu content. Additionally, Pad 1 had both the most significant decrease in cell viability and the highest Cu content, which further testify this statement. Cu is an essential metal in most species but is harmful if uptake is too high (Sterner, 2010). Consequently, BWP from Pad 1 and 2 had the most negative effects due to their high Cu content.

Moreover, the decreasing cell viability can also be linked to the observed ROS production. Since all BWP show sign of ROS production, there is a possibility of causing oxidative stress which has toxic effects on the cells. This resulting ROS formation aligns with the elemental analysis, which shows that BWP from all pads contain possible ROS producing metals, such as Fe, Cu, Cr, Ni, Mn and Ti. However, Pad 1 and Pad 2 had a clearly higher ROS-production for lower particle concentration compared to Pad 3. This could be explained by these BWP being acute cytotoxic, which is supported by the clear decrease in cell viability. As a result, potential cell death at higher concentrations decelerates ROS-formation, causing lower results. Since Pad 3 do not affect cell viability the same way, it has a more linear ROS increase over time and concentration.

Lastly, the non-airborne particles had similar composition as the airborne ones. Even though no cell studies were performed using the non-airborne particles, the comparison between the non-airborne elemental analysis and the airborne cell exposure tests may provide indications of their potential toxicity. Since the non-airborne samples from Pad 1 and 2 contains a similar share of Cu compared to the airborne, they likely also decrease in cell viability as well as ROS production as displayed in the airborne tests. However, Cu and Al are known to be particularly toxic to aquatic species, potentially causing disturbances in reproduction,

metabolism and blood chemistry (Rehman et al., 2019). Therefore, there is a possibility of more intensive toxic effects of non-airborne BWP in aquatic environments compared to airborne ones.

4.4 Uncertainties and Limitations

Firstly, this study is limited by the number of repetitions made. Since only two repetitions were done for the online measurements, they might not be representative enough. Even though the findings still give an indication of the BWP and their effects, more measurement repetitions would increase the credibility of the results.

Moreover, there are particle losses in the online measurements which affect the absolute values of PM and PNC. The losses are mainly expected in the tubes connecting the PoD to the measurement equipment, such as SMPS, CPC and MiniWRAS. Inside these tubes the principles of particle deposition still apply, meaning that particle loss is possible due to sedimentation, impaction and diffusion. The length of the tubes influences sedimentation, as particles may deposit within the tube as the result of a longer distance. Consequently, the deposition and potential loss is higher for larger particles as the settling velocity increases with particle diameter (Equation 1). Additionally, deposition through impaction is greater for tubes with a higher flow and more narrow curves as the inertia of the particle keeps it from following the flow and instead sticks to the tube wall. Diffusion of finer particles within the tubes causes the particles to contact and deposit on the walls. Finally, it is possible for particles to adhere to the tubes because of electrostatic deposition. This phenomenon may be reduced by using metal tubes or electrically conductive tubes (Brockmann, 2011). The tubes used for this study was a combination of both, with an addition of Tygon® tubes. In addition, the sampling lines was kept short to limit sedimentation and without tight curves to limit impaction. These efforts, combined with cleaning between each material, minimized particle losses and contamination of deposited particles. For a comparative study, the effect of particle losses is not substantially affecting the results but needs to be taken into account when discussing the absolute values.

Additionally, the PM concentrations are affected by uncertainties in the MiniWRAS. As discussed in section 4.2, the MiniWRAS usually underestimates the PM concentration when specifically measuring BWP. This is caused by two limitations: the optical diameter and the assumed density. The optical diameter depends on a correct correlation between particle size and scattered light, which is decided by a specific calibration material. If the BWP would scatter less light compared to the calibration material, the particle size would be underestimated, and consequently the PM concentration. Such underestimation of size would also explain the higher share of $PM_{2.5}$ compared to previous literature. This underestimation is pronounced for BWP which usually have higher density than the

assumed standard density, 1g/cm^{3,} (Woo et al., 2021), as examined in section 4.2. Furthermore, since particle size is underestimated, the size distribution would be affected. Nonetheless, the measurements still serve the purpose of this study intended, which is as a comparison between three brake pad types.

Moreover, the size distribution is limited by the long sampling time of the SMPS. Since the SMPS measured over a span of three minutes but only gathered data for certain sizes at a fraction of the time, this means that some spikes or rapid declines could be missed in the data collection process. However, since the data has been averaged over a longer time span and largely matched the MiniWRAS data, the results seem reliable.

Furthermore, there are uncertainties in the cell exposure results. Firstly, handling during transport and testing likely resulted in a loss of particles, such as those sticked to walls of the container or EDXRF dish, which also introduced another uncertainty to the estimated dose for the toxicity experiments. Secondly, experiments may have been affected by the waiting time before the test were carried out. The offline experiment was conducted almost one month after the collection of particles. As the experiment measured ROS, it is possible the compounds in the samples may have lost some of their reactive properties through other reactions, in the time between collection and analysis. However, even if the collection of the three different materials took place on different days, the assumption is that they are still comparable. Nonetheless, this should be taken into consideration if compared to future research on similar materials.

Lastly, the study is limited in the elemental analysis. As previously stated, the EDXRF is a more reliable dedicator for elements with higher atomic numbers. Because of these restrictions, the EDXRF results do not contain all elements present in the BWP, such as oxygen and carbon, and the lighter elements, e.g. Al, might be biased. Therefore, approximation of total weight will likely be lower than the actual one, which subsequently affects the dose-response relationship.

5 Environmental implication

This study has found that the three different brake pads perform differently both in terms of emissions and cellular response. Additionally, differences were also observed when comparing the airborne BWP with the non-airborne. As a result, the environmental impact and effect on human health will be different for the different materials.

The only test where the materials performed similarly was regarding particle size. The resulting number weighted size distributions as well as the mass concentration displayed the emitted main size interval to be $PM_{2.5}$ for all materials. As pointed out by literature, this fine size range is within the respirable fraction which particles have a larger lung deposited surface area and thereby risk causing the more severe health effects compared to larger airborne particles. However, since no clear formation of UFP was observed, the risk of these BWP entering the blood stream is low and thus also the risk of affecting other parts of the body. Despite this, inhaled particles could still cause negative effects in the lungs and airways, which risk increases if the emissions are released in more populated areas. Consequently, BWP from these brake pads are a potential health risk, especially in urban environments.

Since the BWP from the different pad materials are not distinguishable by size, their emitted concentrations become more important. The results show that Pad 1 repeatedly produces the lowest concentrations in terms of both PM_{10} and PNC, while the other two brake pads produce higher concentrations with more irregular behavior, particularly noticeable by the PNC spikes for Pad 3. This difference in results could be explained by the elemental composition of the materials shown in the EDXRF. As seen, Pad 3 BWP contained virtually no Cu, whereas Pad 1 contained the most. Due to the thermal conductivity and ductile properties of Cu, it is known to reduce both PM_{10} concentrations and PNC compared to Cu free brake pads. This aligns with the results of the BWP containing the highest share of Cu came from the pad with the lowest emissions. In addition, the presence of Cu creates more compact and stable secondary plateaus, causing the material to not produce the observed spikes in PNC (Verma et al., 2015). As the BWP from Pad 3 contains the least amount of Cu and presents the most prominent spikes, this is a further support to this finding. Therefore, the presence of Cu is a reasonable explanation for the different performances of the various pads in terms of both PNC and PM_{10} concentration.

However, the results indicate that the BWP that contains more Cu have cytotoxic effects. This means that the brake pad with the lowest emissions, Pad 1, is potentially more toxic, which is shown by the low cell viability. In contrast, the brake pad emitting more particles, Pad 3, showed the weakest sign of cytotoxicity

in the cell exposure tests. It should be noted that the exposure tests used the same BWP concentrations and do therefore not account for the fact that the exposure of Pad 3 emissions is higher. Since it is found that the dose of particles plays an important part, it cannot be excluded that BWP from Pad 3 still have potential negative health effects if respired. As a result, a trade-off between elemental toxicity and emitted concentration can be seen, which raises the question of which property has the largest impact on health and environment.

Moreover, the importance of elemental composition increases when regarding the non-airborne particles. These fast deposited particles potentially end up in water ways, were they could harm aquatic species. Especially Cu and Al, found in the BWP risk erupting reproduction systems, metabolism and blood chemistry, which could potentially lead to negative ecosystem effects. Even though less Al was found in the non-airborne samples, HDV brake pads contain more metal compared to LDV, and have therefore potentially a larger negative impact.

Consequently, there is a question of how to limit these potential negative effects. Since this study did not find substantial UFP, the PM measurement accurately reflects the emitted particle concentration, which testifies the Euro 7 limits values effective tools in restricting the emitted particles. However, Euro 7 does not consider the contrast between emission concentration and elemental toxicity. As a result, it does not regulate the toxic effects from brake pads with low emissions. The question is which particle property should be prioritized in order to limit the most negative environmental effects, or if additional regulation is needed to also take elemental toxicity into account. The risk with the recent PM regulations is that effects from low emission brakes are overlooked.

5.1 Conclusion

In conclusion, this study identifies potential negative environmental impacts and health effects from heavy-duty vehicles brake wear particles. Since the toxicity of the particles is mainly caused by its metal content, especially Cu, heavy-duty vehicles brakes are potentially more toxic compared to light-duty vehicles due to being semi-metallic. However, Cu stabilizes the material and decreases the emission concentrations, which prevents higher dispersion and exposure. Ideally, other metals than Cu should be used to reinforce the brake pads and maintain low emissions. Additionally, the particles were found in the fine, respirable fraction, which makes heavy-duty vehicles a health issue especially in urban areas where the population and exposure is higher. Consequently, the environmental effect depends on both emission concentrations and elemental composition, which suggests that it is not enough to measure and limit only PM in order to limit the actual health impacts.

5.2 Future research

To gain further understanding into the environmental implications of brake particles from heavy-duty vehicles, more research is required. Since this report focused on a specific set of brake pads, it is suggested to continue investigating other types of both brake pads and brake discs. In addition, the results in this paper are impacted by the disc used to generate particles. To confidently make statements about brake wear particles environmental implications explicitly from the brake pads, the disc contribution to the brake wear particles needs to be isolated and excluded.

Furthermore, the toxicity of the brake wear particles can be further investigated. For example, a cell death assay is required to determine cytotoxicity of the brake wear particles. In addition, it would be beneficial to use scanning electron microscopy to further examine the composition and shape of the particles. This also would present the elements chemical form, which deepens the understanding on both toxicity, exposure and dispersion. Moreover, statistical analyses can be performed to confirm the relationship between elemental composition and cell exposure results. Lastly, in vivo studies are required to further link the brake wear particles exposure to the toxic effects.

Additionally, real world scenarios could be investigated more closely. This could be done by testing the effects of thermal fatigue, a process which in real driving has a large influence on brake wear. To test this among other things, dynamometer tests could be performed.

Lastly, to gain a better understanding of how the brake wear particles affect global warming and the issues which follows, measurements of black carbon emissions could be performed.

6 References

Ameziane-El-Hassani, R. and Dupuy, C. (2013). Detection of intracellular reactive oxygen species (CM-H_2DCFDA). *Bio-protocol 3*(1). DOI: 10.21769/BioProtoc.313.

Brockmann, J. E. (2011). Aerosol transport in sampling lines and inlets. In P. Kulkarni, P. A. Baron, K. Willeke (Ed.), *Aerosol measurement: Principles, techniques, and applications* (3rd ed., pp. 68-105). John Wiley & Sons Inc. https://doi.org/10.1002/9781118001684.ch6

Brouwer, D. H., Lidén, G., Asbach, C., Berges, G. M., van Tongeren, M. (2014). Monitoring and sampling strategy for (manufactured) nano objects, agglomerates and aggregates (NOAA): Potential added value of the nanodevice project. In U. Vogel, K. Savolainen, W. Qinglan, M. van Tongeren, D. Brouwer, M. Berges (Ed.) *Handbook of nanosafety.* (pp. 173-206). Academic Press https://doi.org/10.1016/B978-0-12-416604-2.00005-6

Christou A, Giechaskiel B, Olofsson U, Grigoratos T. Review of health effects of automotive brake and tyre wear particles. *Toxics*. *13*(4) 10.3390/toxics13040301.

Couval, R., Bard, L., Olofsson, U. (2026) Particulate matter from standard heavy duty vehicles mechanical brakes: a multiparameter ranking approach. *Wear, 594*. https://doi.org/10.1016/j.wear.2026.206650

Dekati. (n.d.). *Dekati® gravimetric impactors product range.* Available at: dekati-gravimetric-impactor-product-range-2025.pdf. (2026.02.04)

Directive 2024/2881. *European Parliament and of the Council of 23 October 2024 on ambient air quality and cleaner air for Europe* Available at: https://eur-lex.europa.eu/legal-content/EN/TXT/?uri=OJ:L_202402881

Durag group. (n.d.) *Portable wide-range aerosol spectrometer.* Available at: https://www.durag.com/en/product-filter-837.htm?productID=MiniWRAS%201371 (2026.03.20)

EEA. (2025). *Emissions of air pollutants from transport in Europe*. Available at: https://www.eea.europa.eu/en/analysis/indicators/emissions-of-air-pollutants-from (2026.03.09)

EIT Urban Mobility. (2025). *Study on non-exhaust emissions in road transport.* Available at: https://www.eiturbanmobility.eu/wp-content/uploads/2025/05/41-EIT-Emissions-Report-5a-Digital-1.pdf [PDF]

European Commission. (2014). *Questions and answers on the commission strategy for reducing heavy-duty vehicles' (HDVs) fuel consumption and CO2 emissions.* Available at: https://ec.europa.eu/commission/presscorner/detail/en/memo_14_366 (2026.02.11)

Gramstat, S., Mertens, T., Waninger, R., Lugovyy, D., Impacts on brake particle emission testing. *Atmosphere, 11*(10), 1132. https://doi.org/10.3390/atmos11101132

Grigoratos, T., Martini, G. (2015). Brake wear particle emissions: a review. *Environmental science pollution research* ,*22*, 2491–2504. https://doi.org/10.1007/s11356-014-3696-8

Harrison, RM,. Allan, J., Carruthers, D., Heal, MR., Lewis, AC., Marner, BB., Murrells, T. & Williams, A. (2021). Non-exhaust vehicle emissions of particulate matter and VOC from road traffic: A review. *Atmospheric environment*. *262*. https://doi.org/10.1016/j.atmosenv.2021.118592

Hinds, W. C. (1999). *Aerosol technology: Properties, behaviour and measurement of airborne particles*. (2nd ed). John Wiely and sons.

Hussain, S., Abdul Hamid, M.K, Mat Lazim, A.R., & Abu Bakar, A.R. (2014). Brake wear particle size and shape analysis of non-asbestos organic (NAO) and semi metallic brake pad. *JurnalTeknologi.* Available at: https://journals.utm.my/jurnalteknologi/article/view/3731/2740. (2026.03.09)

Järlskog, I. Gustavsson, M. (2023) Traffic: an environmental problem that just keeps rolling on. In K. Djerf (Ed.), *Air and environment: air quality and Swedish air quality monitoring* (pp. 48-53). Swedish EPA. ISBN 978-91-620-1309-7

Kamiloglu, S., Sari, G., Ozdal, T., Capanoglu, E. (2017). Guidelines for cell viability assays. *Food frontiers. 1*(3), 332-349. https://doi.org/10.1002/fft2.44

Karlsson, H. (2023). Toxicology: a way of understanding particles. In K. Djerf (Ed.), *Air and environment: air quality and Swedish air quality monitoring* (pp. 42-47). Swedish EPA. ISBN 978-91-620-1309-7

Kenelec. (2014). *Fundamentals of condensation particle counters (CPC) and scanning mobility particle sizer (SMPS) spectrometers.* https://www.kenelec.com.au/wp-content/uploads/2018/04/-CPC-003-Fundamentals-of-Condensation-Particle-Counters-and-Scanning-Mobility-Particle-Sizer-Spectrometers-AppNote.pdf (2026.01.26)

Lopez, B., Wang, X., Chen, A. L.-W., Ma, T., Mendez-Jimenez, D., Cobb, L.C., Frederickson, C., Fang, T., Hwang, B., Shiraiwa, M., Park, M., Park, K.,

Yao, Q., Yoon, S & Jung, H. (2023). Metal contents and size distributions of brake and tire wear particles dispersed in the near-road environment. *Science of the total environment, 883.* https://doi.org/10.1016/j.scitotenv.2023.163561

Lundin, J. (2024). *Investigation of brake wear particle emissions from heavy-duty vehicles*. [Master's Thesis, LTH Faculty of engineering]. Available at: http://lup.lub.lu.se/student-papers/record/9154406

Lyu, Y., Leonardi, M., Wahlström, J., Gianella, S., Olofsson, U. (2020) Friction, wear and airborne particle emission from Cu-free brake materials. *Tribology international, 141*. https://doi.org/10.1016/j.triboint.2019.105959

Lyu, Y., Varriale, F., Malmborg, V., Ek, M., Pagels, J., Wahlström, J. (2024) Tribology and airborne particle emissions from grey cast iron and WC reinforced laser cladded brake discs. *Wear, 556-557*. https://doi.org/10.1016/j.wear.2024.205512

Lyu, Y., Zhang, Q., Tanzeglock, L., Tu, M., Mo, J., Okuda, T., Pagels, J., Wahlström, J. (2025). Mapping of friction, wear and particle emissions from high-speed train brakes. *Wear, 572-573,* https://doi.org/10.1016/j.wear.2025.206027

Molecular Probes, Inc. (2006). *Reactive Oxygen Species (ROS) detection reagents* (Manual MP 36103). Invitrogen Corporation. https://assets.fishersci.com/TFS-Assets/LSG/manuals/mp36103.pdf

Neukirchen, C., Saraji-Bozorgzad, M.R., Mäder, M., Mudan, A.P., Czasch, P., Becker, J., Di Bucciano, S., Trapp, C., Zimmerman, R. & Adam, T. (2025). Comprehensive elemental and physical characterization of vehicle brake wear emissions from two different brake pads following the Global Technical Regulation methodology. *Journal of Hazardous Materials, 482.* https://doi.org/10.1016/j.jhazmat.2024.136609

Regulation (2024/1257). *European Parliament and of the Council (EU) of 24 April 2024 on type-approval of motor vehicles and engines and of systems, components and separate technical units intended for such vehicles, with respect to their emissions and battery durability (Euro 7)* Available at: https://eur-lex.europa.eu/eli/reg/2024/1257/oj/eng

Rehman, M., Liu, L., Wang, Q., Hamzah Saleem, M., Bashir, S., Ullah, S., Peng, D. (2019) Copper environmental toxicology, recent advances , and future outlook: a review. *Environmental Science and Pollution Research 26*, pp. 18003-18016. https://link.springer.com/article/10.1007/s11356-019-05073-6#Sec3

Rigaku. *(n.d.). What Is EDXRF Spectroscopy?.* Available at: https://rigaku.com/products/xrf-spectrometers/edxrf/technique (2026.01.26).

Rigaku. (2025) *What XRF can and can´t analyze: A guide for beginners.* Available at*:* https://rigaku.com/products/xrf-spectrometers/learning/blog/what-xrf-can-and-cannot-analyze-a-guide-for-beginners (2026.05.06).

Salama, A.I.A. (2000). Mechanical techniques: particle size separation. In I.D. Wilson. (Ed.), *Encyclopedia of Separation Science.* (pp.3277-3289). Academic press. https://doi.org/10.1016/B0-12-226770-2/07641-9

Seville, J & Wu, Chuan-Yu. (2016). *Particle Technology and Engineering: An Engineer's Guide to Particles and Powders: Fundamentals and Computational Approaches.* Butterworth-Heinemann. pp. 39-65. https://doi.org/10.1016/B978-0-08-098337-0.00003-5

Sjöberg, K., Söderlund, K., Swietlicki, E., Kristensson, A., Krejci, R. (2023). What are particles and how do they affect us? In K. Djerf (Ed.), *Air and environment: air quality and Swedish air quality monitoring* (pp. 6-11). Swedish EPA. ISBN 978-91-620-1309-7

Straffelini, G, Ciudin, R., Ciotti, A., Gialanella, S. (2015). Present knowledge and perspectives on the role of copper in brake materials and related environmental issues: A critical assessment. *Environmental Pollution, 207*, 211-219. https://doi.org/10.1016/j.envpol.2015.09.024

TSI Incorporated. (2022a) *Scanning mobility particle sizer spectrometer model 3938* (Document No. 5001531). Incorporated. https://.com/getmedia/6417ff18-99f7-4e15-8eed-971c92f1052c/SMPS-3938_US_5001531_RevE_Web?ext=.pdf

TSI Incorporated. (2022b) *Condensation particle counter model* 3752 (Document No. 5002014). Incorporated. https://.com/getmedia/6cb581a9-e0bd-4958-8b87-0666b4a80606/3752_A4_5002014_RevB_Web?ext=.pdf

Perricone, G., Matejka, V., Alemani, M., Wahlström, J., Olofsson, U. (2019). A test stand study on the volatile emissions of a passenger car brake assembly. *Atmosphere (10).* 10.3390/atmos10050263

Präbst, K., Engelhardt, H., Ringgeler, S., Hübner, H. (2017). Basic colorimetric proliferation assays: MTT, WST, and Resazurin. In D. Gilbert & O. Friedrich (Ed.) *Cell Viability Assays. Methods in Molecular Biology* (pp. 1-17). Humana Press, New York, NY. https://doi.org/10.1007/978-1-4939-6960-9_1

United States Environmental Protection Agency. (2025, 6 June). *What is particle pollution?* https://www.epa.gov/pmcourse/what-particle-pollution

Verma, P.C., Menapace, L., Bonfanti, A., Ciudin, R., Gialanella, S., Straffelini, G. (2015). Brake pad-disc system: Wear mechanisms and formation of wear fragments. *Wear, 322-323* https://doi.org/10.1016/j.wear.2014.11.019

Wahlström, J., Lyu, Y., Lundberg, J., Pagels, J., Hjelm, R. (2025). Advancing tyre and road wear particle measurements: balancing laboratory conditions and real-world relevance. *Atmosphere, 16*(5) https://doi.org/10.3390/atmos16050588

Wahlström, J., Lyu, Y., Matjeka, V., Söderberg, A. (2017). A pin-on-disc tribometer study of disc brake contact pairs with respect to wear and airborne particle emissions. *Wear, 384-385*, pp.124-130. https://doi.org/10.1016/j.wear.2017.05.011

Wahlström, J. (2011). *A study of airborne wear particles from automotive disc brakes.* [Doctoral thesis, KTH Royal Institute of Technology]. Industrial Engineering and Management, KTH Royal Institute of Technology. https://doi.org/10.13140/rg.2.1.4751.5681.

Wang, Y., Shuai, S., Ge, Y. (2025). Controlling brake particle emissions: new brake disc needs more attention. *Results in engineering, 27.* https://doi.org/10.1016/j.rineng.2025.107120

Woo, S., Kim, Y., Lee, S., Choi, Y., Lee, S. (2021) Characteristics of brake wear particle (BWP) emissions under various test driving cycles. *Wear, 480-481*. https://doi.org/10.1016/j.wear.2021.203936

World Health Organization. (2024). *Ambient (outdoor) air pollution*. https://www.who.int/news-room/fact-sheets/detail/ambient-(outdoor)-air-quality-and-health

Yang, L., Nishita-Hara, C., Shiraishi, M., Tsubakida, K., Shibata, Y., Jing, W., Li, D., Yoshimura, K., Kurokawa, N., Hotta, A., Okuda, T. (2026). Developement of a water-soluble filter for potential use in toxicity evaluation of ambient particulate matter. *Aerosol and air quality research 26*(6). https://doi.org/10.1007/s44408-025-00082-2

Appendix A Brake mechanics

This section presents the mechanical relationships and calculations used in Pin on Disc experiments

An important relation in disc brake systems is between the angular velocity of the disc and the wheel. The angular velocity of a wheel can be calculated using the velocity of the vehicle and the wheels radius, as seen in Equation 2. The same is true for the angular velocity of the brake disc (Equation 3). As the angular velocity of the two is the same, Equations 2 and 3 can be combined and rearranged into Equation 4 and used to find the sliding velocity. The sliding velocity is the velocity of the disc.

$$\omega_{wheel} = \frac{v_{truck}}{r_{wheel}} \tag{2}$$

$$\omega_{disc} = \frac{v_{sliding}}{r_{disc}} \tag{3}$$

$$v_{sliding} = \frac{v_{truck}}{r_{wheel}} x\, r_{disc} \tag{4}$$

To calculate the sliding velocity in the form of rounds per minute (rpm), the following equation is used.

$$n = \frac{v_{sliding}}{r_{disc}} x \frac{60}{2\pi} \tag{5}$$

Appendix B Online data

This section contains data from all measurement repetitions made by MiniWRAS, CPC and SMPS.

B.1 PM_{10} (MiniWRAS)

B.1.1 PM_{10} concentration repetitions

The following figures (Figure 28- Figure 30) show all repetitions of recorded PM_{10} concentration for all pads. The figures display the average of the two repetitions (labelled P1, P2 or P3). Like in the previous section the individual repetitions are labelled with both number and letters. The letter corresponds to the setting i.e. 'E' corresponds to the extreme setting, and '1' being the first run out of two.

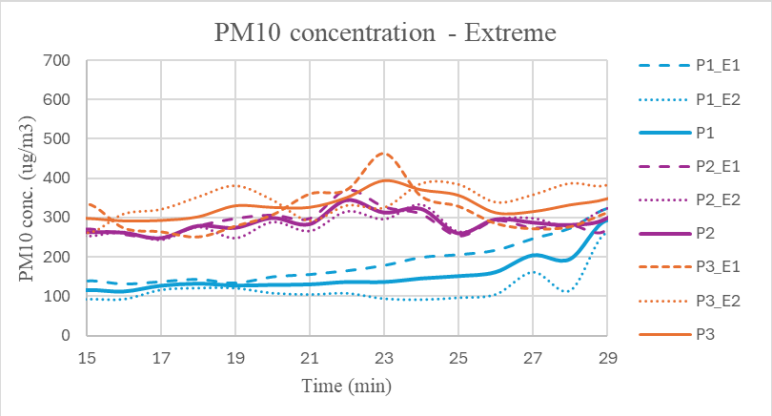


Figure 28: PM_{10} concentration at 2500 rpm for all three pads, presenting both the two runs and the average.

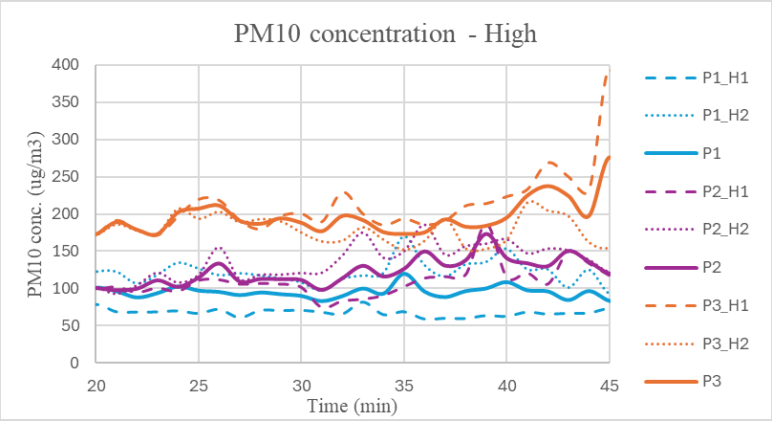


Figure 29: PM_{10} concentration at 1900 rpm for all three pads, presenting both the two runs and the average

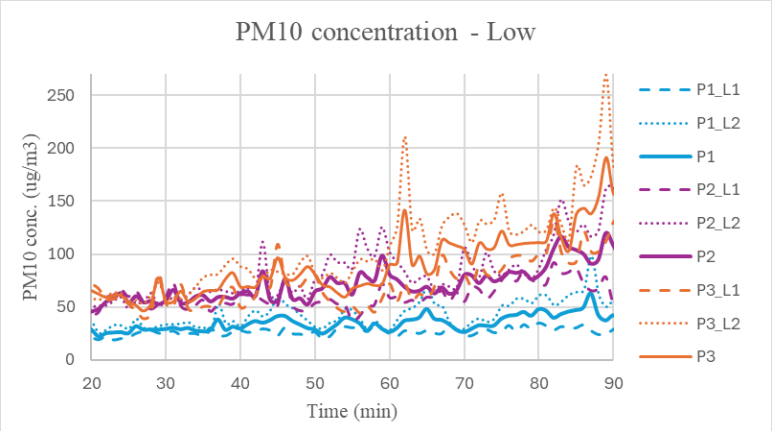


Figure 30: PM_{10} concentration at 1100 rpm for all three pads, presenting both the two runs and the average.

B.1.2 Calculation of average PM_{10} concentration based on sample mass

To investigate the validity of the MiniWRAS PM_{10} concentration results, the average PM_{10} concentration based on the mass sampled on the filters was performed using Equation 6. Where the concentration can be calculated using m, which is the total sampled filter mass, F is the flow through the impactor, and t is the total duration of sampling.

$$C = \frac{m}{F \times t} \tag{6}$$

Total duration of sampling, t:

$$180 \text{ min}(1100\ rpm) \times\ 2 + 40 \text{ min } (1900\ rpm)\ \ \times 8 = 680\ min$$

Sampled filter mass, m:

Pad 1: 8,05 mg

Pad 2: 11,52 mg

Pad 3: 13,94 mg

Flow through impactor, F:

30 l/ min

B.2 Particle number concentration (CPC)

The following figures (Figure 31-Figure 33) show all repetitions of recorded data of PNC for all pads. The figures display the average of the two repetitions (labelled P1, P2 or P3). The repetitions are labelled with both number and letters. The letter corresponds to the setting i.e. 'E' corresponds to the extreme setting, and '1' being the first run out of two.

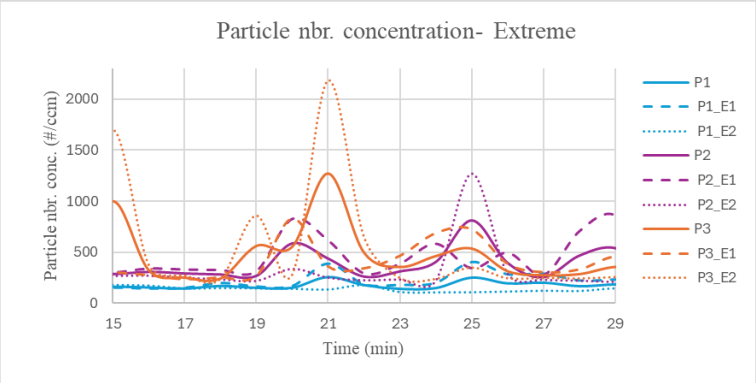


Figure 31: PNC at 2500 rpm for all three pads, presenting both the two runs and the average.

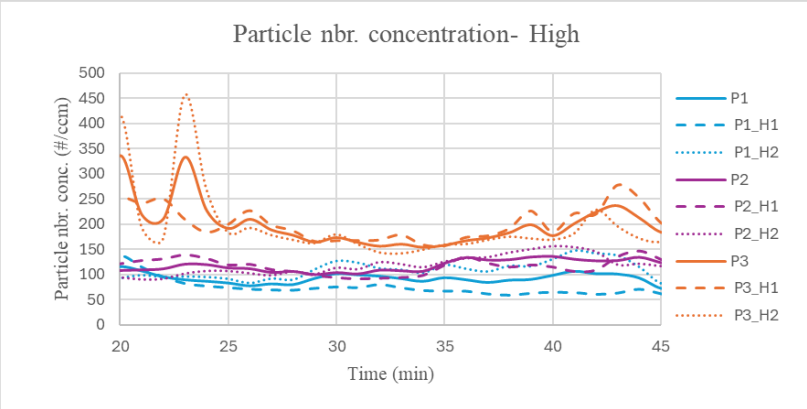


Figure 32: PNC at 1900 rpm for all three pads, presenting both the two runs and the average.

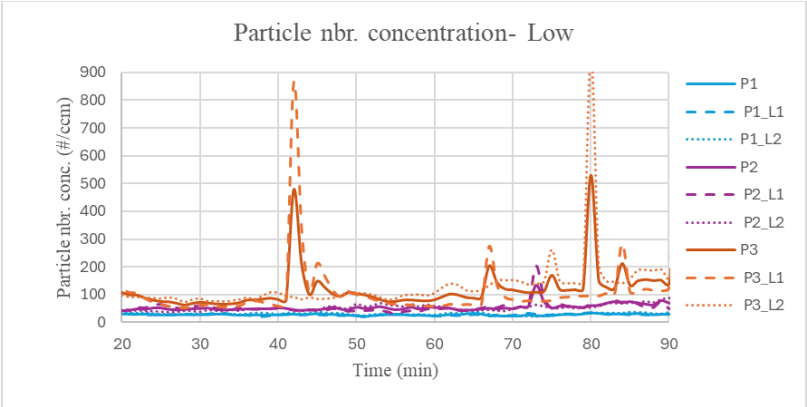


Figure 33: PNC at 1100 rpm for all three pads, presenting both the two runs and the average.

B.3 Particle size distribution (MiniWRAS & SMPS)

B.3.1 Particle size distribution repetitions

To present the size distribution data in a matter where all repetitions are readable, the data from the SMPS and the MiniWRAS has, unlike in section 4.2.3, been displayed separately. The data from the SMPS is shown in Appendix B.3.11 and the MiniWRAS data in Appendix B.3.1.2.

The following figures (Figure 34-Figure 39) show all repetitions of recorded size distribution for all pads. The figures display the average of the two repetitions (labelled P1, P2 or P3). Like in the previous section the individual repetitions are

labelled with both number and letters. The letter corresponds to the setting i.e. ‘E’ corresponds to the extreme setting, and ‘1’ being the first run out of two.

B.3.1.1 SMPS repetitions

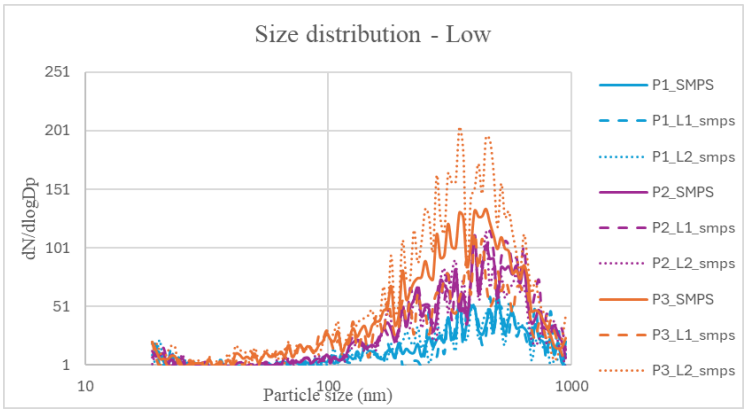


Figure 34: Size distribution at 1100 rpm for all three pads, presenting both the two runs and the average. Only SMPS data included.

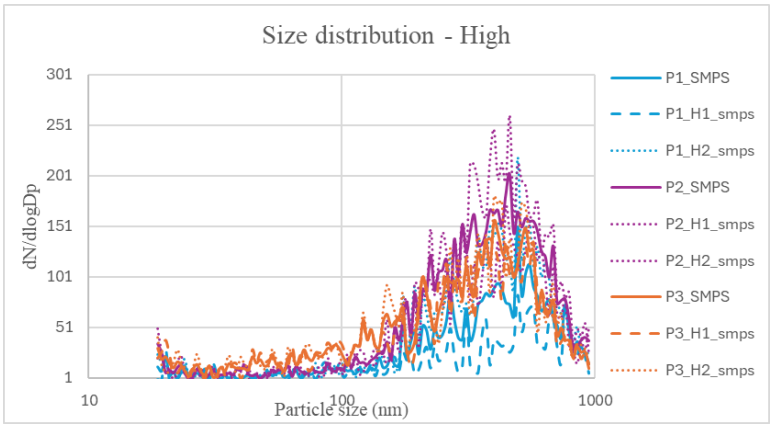


Figure 35: Size distribution at 1900 rpm for all three pads, presenting both the two runs and the average. Only SMPS data included.

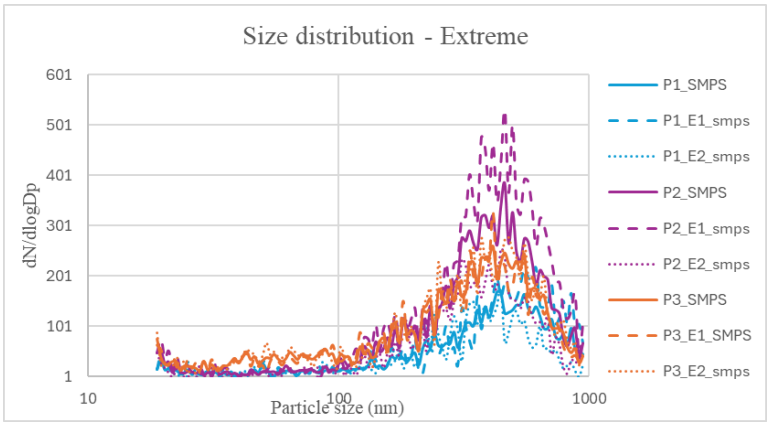


Figure 36: Size distribution at 2500 rpm for all three pads, presenting both the two runs and the average. Only SMPS data included.

B.3.1.2 MiniWRAS repetitions

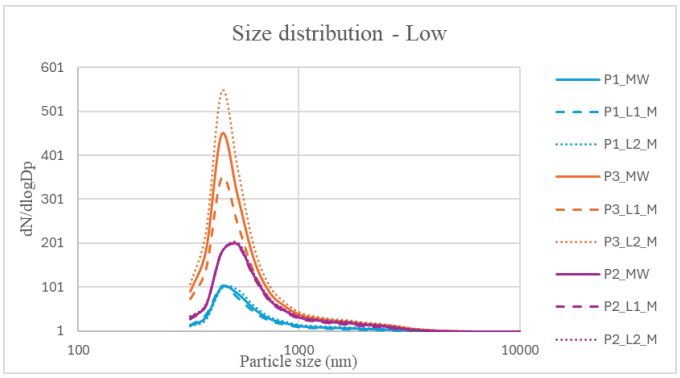


Figure 37: Size distribution at 1100 rpm for all three pads, presenting both the two runs and the average. Only MiniWRAS data included.

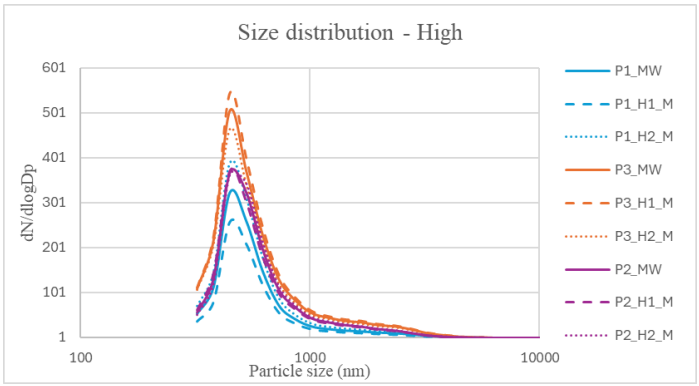


Figure 38: Size distribution at 1900 rpm for all three pads, presenting both the two runs and the average. Only MiniWRAS data included.

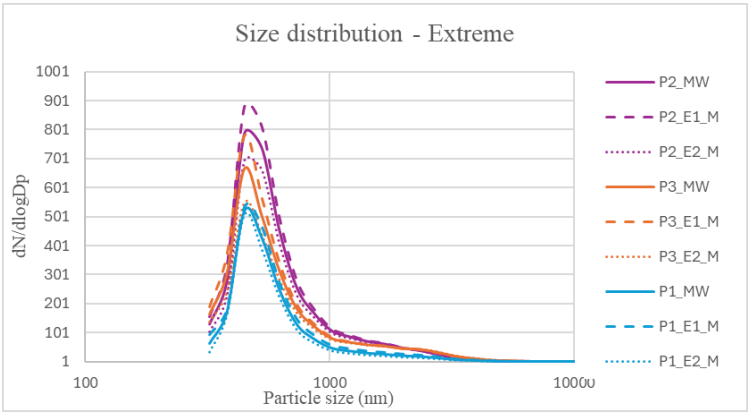


Figure 39: Size distribution at 2500 rpm for all three pads, presenting both the two runs and the average. Only MiniWRAS data included.

B.3.2 Size distribution analysis of PNC peaks

The PNC results presented in Figure 18 shows that Pad 3 BWP generated noticeable spikes. By selecting the times which showed peaks and studying these occurrences using the MiniWRAS and SMPS data the size distribution was further analysed. The MiniWRAS showed no changes for any of these incidences, indicating that the spike in PNC was likely due to an increase in the finer particle sizes. The SMPS data was mainly identical to the averages shown in Figure 21-Figure 23, except for one instance. The SMPS results at this time compared for the averages of the same pad and setting are presented in Figure 40. As can be seen the size distribution at this time shows that the amount of ultrafine particles are much higher when compared to the average.

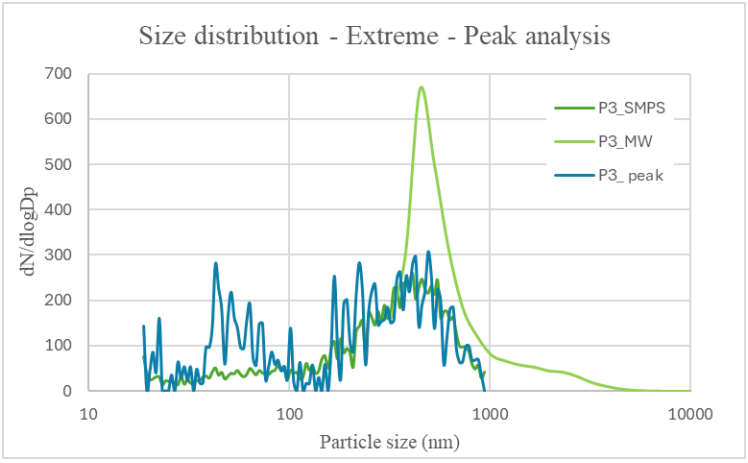


Figure 40: Size distribution from one of the repetitions of Pad 3 SMPS during a peak, compared to the average of Pad 3 BWP. Average SMPS data is presented in light green, the averaging MiniWRAS data in dark green and the SMPS data collected at the time of the spike in blue. All at extreme condition (2500 rpm).

Appendix C Metal composition of particles (EDXRF)

C.1 Relative elemental composition. Water soluble filter with airborne particles.

Table 11: Relative elemental composition of airborne BWP from Pad 1, 2 and 3.

Element (%)	Transport Blank	Total Blank	Airborne		
			Pad 1	Pad 2	Pad 3
Mg	0,60	0,44	3,39	1,58	1,03
Al	1,61	0,45	3,60	10,65	8,71
Si	4,15	6,05	2,16	2,12	1,63
P	0,00	0,29	0,06	0,64	0,04
S	61,07	67,68	1,44	1,27	0,90
Cl	0,63	0,00	0,09	0,03	0,05
K	0,92	15,43	−0,01	0,25	−0,01
Ca	4,15	4,89	3,70	2,43	5,49
Ti	0,46	0,31	0,39	0,00	0,00
V	0,00	0,00	0,00	0,04	0,10
Cr	0,80	0,25	1,96	0,70	6,35
Mn	0,22	0,00	0,47	0,44	0,43
Fe	19,80	1,53	68,18	58,50	73,92
Ni	0,82	0,25	0,07	0,04	0,07
Cu	2,64	1,14	13,82	9,24	0,76
Zn	2,13	0,92	0,65	12,03	0,49
As	0,00	0,00	0,00	0,00	0,00
Se	0,00	0,00	0,00	0,00	0,00
Pb	0,00	0,00	0,04	0,04	0,04

C.2 Relative elemental composition. Teflon filter with non-airborne particles.

Table 12: Relative elemental composition of non-airborne BWP from Pad 1, 2 and 3.

Element (%)	Transport Blank	Total Blank	Non-airborne		
			Pad 1	Pad 2	Pad 3
Mg	0,00	0,00	0,88	0,38	0,24
Al	7,47	8,42	1,17	3,63	3,95
Si	3,35	3,63	0,74	0,93	0,92
P	7,47	7,11	0,01	0,42	0,00
S	0,00	0,00	0,89	1,10	0,91
Cl	0,00	0,00	0,00	0,00	0,00
K	0,00	0,00	0,00	0,09	0,00
Ca	26,22	24,96	2,74	1,61	6,12
Ti	3,43	2,76	0,24	0,00	0,00
V	0,00	0,00	0,05	0,00	0,06
Cr	0,00	0,00	1,92	0,66	7,06
Mn	0,00	0,00	0,52	0,49	0,45
Fe	9,15	11,18	73,24	65,58	79,45
Ni	14,86	15,24	0,07	0,04	0,08
Cu	20,58	19,59	16,72	10,17	0,42
Zn	13,41	12,19	0,76	14,78	0,12
As	0,00	0,00	0,00	0,00	0,00
Se	0,00	0,00	0,00	0,00	0,00
Pb	0,00	0,00	0,05	0,12	0,20

Appendix D Cell exposure data

D.1 Cell viability data

D.1.1 Calculations of relative cell viability

This section presents the data from WST-1 assay and the calculations of relative cell viability.

The relative cell viability is calculated using Equation 7. To calculate this, the measured absorbance is firstly used to calculate one average for each column of pink blank wells below the pad samples (sample blank) and one average for the four pink blank wells below the control sample (control blank), Figure 41. The cell viability is found by then subtracting the average sample blank from each sample measurement and dividing this with the subtraction of control absorbance with the average control blank.

$$Relative\ cell\ viabilty = \frac{ABS_{Sample} - ABS_{avg(Sample\ blank)}}{avg(ABS_{Control} - ABS_{avg(Control\ blank)})} \times 100 \quad (7)$$

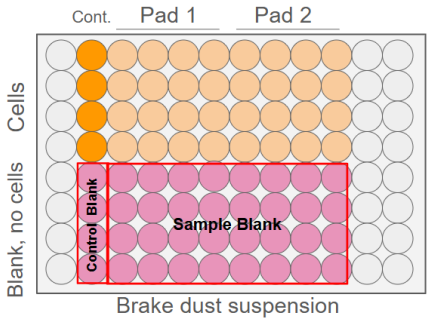


Figure 41: Theoretical display of the resulting WST-1 plate, illustrating the different types of blank wells.

D.1.2 WST-1 assay results, n=4

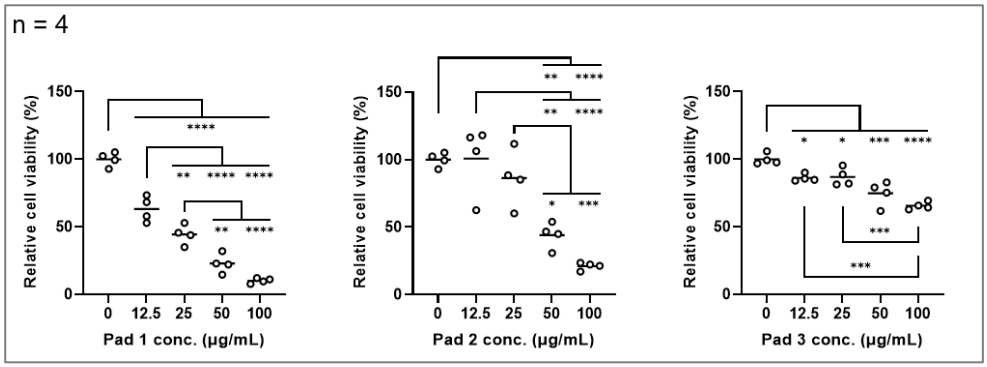


Figure 42: WST-1 assay results of pad 1, 2 and 3 using measurements from all wells i.e. n=4.

D.2 ROS production data, n=4

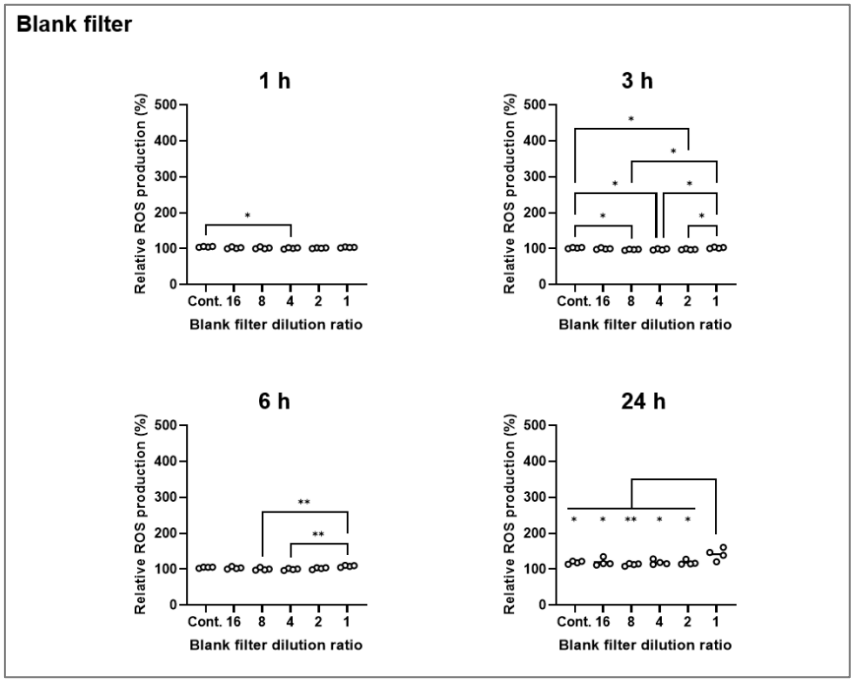


Figure 43: Relative ROS production of blank filter, for 1, 3, 6 and 24 hours, using measurements from all wells i.e. n=4.

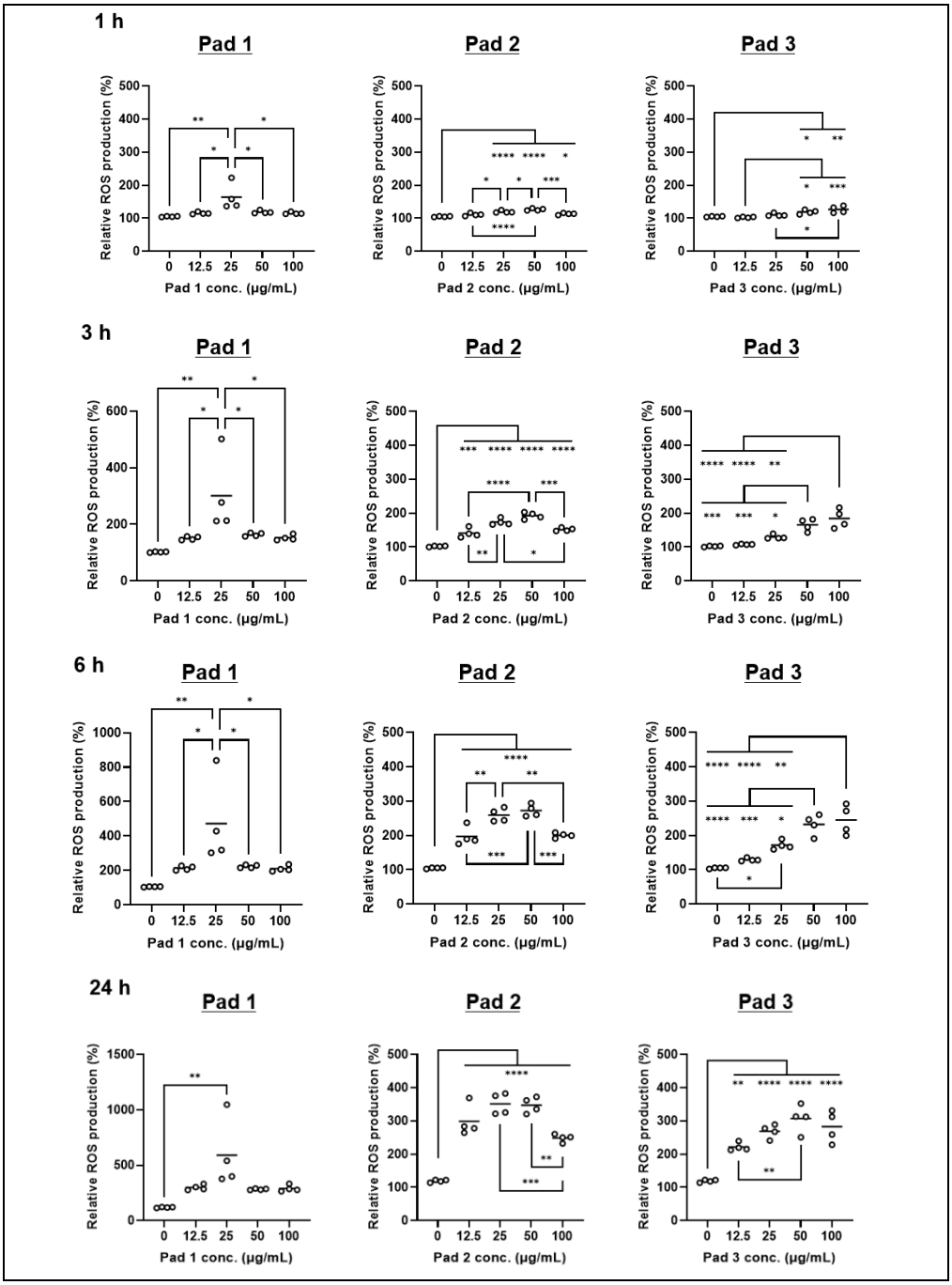


Figure 44: ROS production results of all three pads at 1, 3, 6, 24 hours, using measurements from all wells i.e. n=4.